European Journal of Medicinal Chemistry 128 (2017) 107–122

Contents lists available at ScienceDirect

European Journal of Medicinal Chemistry

journal homepage: http://www.elsevier.com/locate/ejmech

Research paper

Naphthalene diimide-polyamine hybrids as antiproliferative agents: Focus on the architecture of the polyamine chains

Andrea Milelli [a, *], Chiara Marchetti [b], Maria Laura Greco [c], Federica Moraca [d], Giosuè Costa [d], Eleonora Turrini [a], Elena Catanzaro [a], Nibal Betari [a], Cinzia Calcabrini [a], Claudia Sissi [c], Stefano Alcaro [d], Carmela Fimognari [a], Vincenzo Tumiatti [a], Anna Minarini [b]

[a] Department for Life Quality Studies, Alma Mater Studiorum-University of Bologna, 47921 Rimini, Italy
[b] Department of Pharmacy and Biotechnology, Alma Mater Studiorum-University of Bologna, 40126 Bologna, Italy
[c] Department of Pharmaceutical and Pharmacological Sciences, University of Padova, 35131 Padova, Italy
[d] Dipartimento di Scienze della Salute, Università 'Magna Græcia' di Catanzaro, 88100 Catanzaro, Italy

ARTICLE INFO

Article history:
Received 15 December 2016
Received in revised form
18 January 2017
Accepted 19 January 2017
Available online 22 January 2017

Keywords:
Naphthalene diimides
Drug design
DNA
G-quadruplex
Telomeric DNA
Topoisomerase
Antiproliferative

ABSTRACT

Naphthalene diimides (NDIs) have been widely used as scaffold to design DNA-directed agents able to target peculiar DNA secondary arrangements endowed with relevant biochemical roles. Recently, we have reported disubstituted linear- and macrocyclic-NDIs that bind telomeric and non-telomeric G-quadruplex with high degree of affinity and selectivity. Herein, the synthesis, biological evaluation and molecular modelling studies of a series of asymmetrically substituted NDIs are reported. Among these, compound **9** emerges as the most interesting of the series being able to bind telomeric G-quadruplex ($\Delta Tm = 29\ ^{\circ}C$ at 2.5 μM), to inhibit the activity of DNA processing enzymes, such as topoisomerase II and TAQ-polymerase, and to exert antiproliferative effects in the NCI panel of cancer cell lines with GI_{50} values in the micro-to nanomolar concentration range (*i.e.* SR cell line, $GI_{50} = 76$ nM). Molecular mechanisms of cell death have been investigated and molecular modelling studies have been performed in order to shed light on the antiproliferative and DNA-recognition processes.

1. Introduction

Naphthalene diimides (NDIs) represent a class of electron-deficient aromatic compounds widely used in the field of supramolecular and material chemistry [1]. In the last years, this scaffold has been exploited in the design of biologically active compounds. In particular, published reports highlighted the use of NDI as optical imaging probe [2] and, in the medicinal chemistry field, as potential drug candidates. Indeed, several NDIs are able to inhibit enzymes, such as acetylcholinesterase [3], or to exert remarkable antiproliferative activities [4,5] through different mechanisms of action among which intercalation within double-stranded DNA (dsDNA) [6] and stabilization of higher order DNA secondary structures are worth of mention [7]. Over the years, dsDNA has represented the prominent target in the design of new anticancer agents; however, dsDNA-directed molecules suffer from different drawbacks, such as low selectivity towards non-cancerous cells [8]. Recently, other secondary DNA arrangements endowed with relevant biological roles have been discovered, notably the G-quadruplex structures [7]. Guanine-rich DNA sequences, located in distinct regions of the genome, such as oncogene promoters and telomeric regions, can assemble into G-quadruplex. Molecules able to stabilize these secondary structures, located at telomeric ends, prevent the binding of telomerase enzyme leading to senescence and cell death, while stabilization of G-quadruplex located in the promoter region of oncogenes results in a down-regulation of the expression of these genes [9,10]. Further, it is important to point out that G-quadruplex are significantly more prevalent in tumor tissues

Abbreviations: BASASA, Boltzmann Accessible Solvent Accessible Surface Area; BCL-2, B-cell lymphoma 2; dsDNA, double-stranded DNA; hTel, human telomeric; HSP90, heat shock protein 90; MD, Molecular Dynamics; MC, Monte Carlo method; NDI, Naphthalene Diimide; PARP, poly(ADP)ribose polymerase; SASA, Solvent Accessible Surface Area.

* Corresponding author.
E-mail address: andrea.milelli3@unibo.it (A. Milelli).

http://dx.doi.org/10.1016/j.ejmech.2017.01.025
0223-5234/

compared to non-transformed cells [11].

A large number of molecules able to stabilize both telomeric and promoter G-quadruplex have been reported in the last years and a large number of them shares similar structural features, that is a large planar (hetero)aromatic core decorated with two or more harms carrying positively charged nitrogen(s) extremely favorable in the quadruplex recognition process [12]. NDIs have been extensively explored as scaffold for the design of G-quadruplex binders [13–16]. Indeed, it can be easily subjected to different types of core functionalization, thus allowing diverse structural modifications leading to di-, tri- and tetra-substituted derivatives [1,17]. In this context, a number of tetra-substituted NDIs have been developed by Neidle's group: in particular, compound **1** (Fig. 1) stabilizes several distinct DNA quadruplex sequences, such as hTel, HSP90 A and B, BCL-2 and k-RAS [18]. Moreover, **1** has significant *in vivo* antitumor activity in a MIA PaCa-2 pancreatic cancer xenograft model. Compound **2**, developed by Richter and co-workers, represents an example of tri-substituted NDI that displays stabilization of hTel and antiproliferative effects in colon (HT29), lung (A549) and melanoma (SKMel-5) tumor cells [19].

As part of our drug discovery program, we have recently reported some symmetrically di-substituted NDIs endowed with remarkable antiproliferative activities. Compound **3** (Fig. 1), bearing 2-methoxybenzylpropylendiamine side chains, strongly binds DNA and induces apoptotic cell death. Compound **3** was subject to an optimization campaign aimed at improving its pharmacological profile [16,20]. Among the new derivatives, compounds **4** and **5** (Fig. 1) emerged as potent G-quadruplex binders. Compound **4**, bearing 2,3,4-trimethoxybenzylpropylendiamine chains, is cytotoxic in a large panel of cancer cell lines thank to a simultaneous interaction with different biological targets among which the interaction with telomeric G-quadruplex is worth of mention [20]. Macrocyclic analogue **5** strongly stabilizes hTel and c-Kit quadruplex sequences with a good level of selectivity for G-quadruplex over dsDNA [16]. Unfortunately, in spite of these encouraging properties, compound **5** has weaker antiproliferative effects compared to compounds **3** and **4**.

From biophysical analysis and molecular modelling studies performed on these disubstituted and macrocyclic NDIs emerged that G-quadruplex binding property strongly depend on a) the length of the polymethylene linker separating the nitrogen atom(s) of the lateral chains mounted on the NDI nucleus, b) the number of the nitrogen atoms of the lateral chains and c) the nature of the substituent on aromatic rings of the lateral chains. Furthermore, molecular modelling studies point out that the NDI-DNA recognition process is driven by the establishment of both electrostatic and hydrophobic interactions involving both NDI core and peripheral substituted aromatic ring.

Based on these premises, we attempted to increase the cytotoxic activity of NDIs towards cancer cells by merging the best features of the compounds obtained so far focusing on G-quadruplex. To this aim, we designed asymmetric substituted NDIs where one arm was constituted by a substituted-benzylpropylendiamine and the other harm was constituted by a polyaminechain. Indeed, it is well known that polyamines are able to establish strong interactions with biological counterparts due to their positively charged nitrogen atoms. The interaction of polyamines (*i. e.* spermine) on G-quadruplex has been recently confirmed, evidencing different effects on the tetrahelical stability, according to their concentration [21,22]. In addition, it is well established that the polyamine's uptake by the polyamine transport system, which is overactive in cancer cells, contributes to the increased antiproliferative activity of some anticancer agents conjugate with polyamines [23].

In order to identify the most favorable substituent on the aromatic ring of the side chain, in terms of G-quadruplex recognition, 2-methoxybenzylpropylendiamine-NDI-spermine (**6**) and 2,3,4-trimethoxybenzylpropylendiamine-NDI-spermine (**7**) were designed as prototypes (Fig. 2). After a preliminary evaluation, the most efficient hit for the stabilization of the G-quadruplex form of hTel (compound **6**, see later), was modified in the polyamine chain by varying the length of the chain, the number of nitrogen atoms and the distance between them. To this aim, both natural and non-natural polyamines were employed.

In particular, we synthesized derivatives: *i*) **8**–**10** characterized

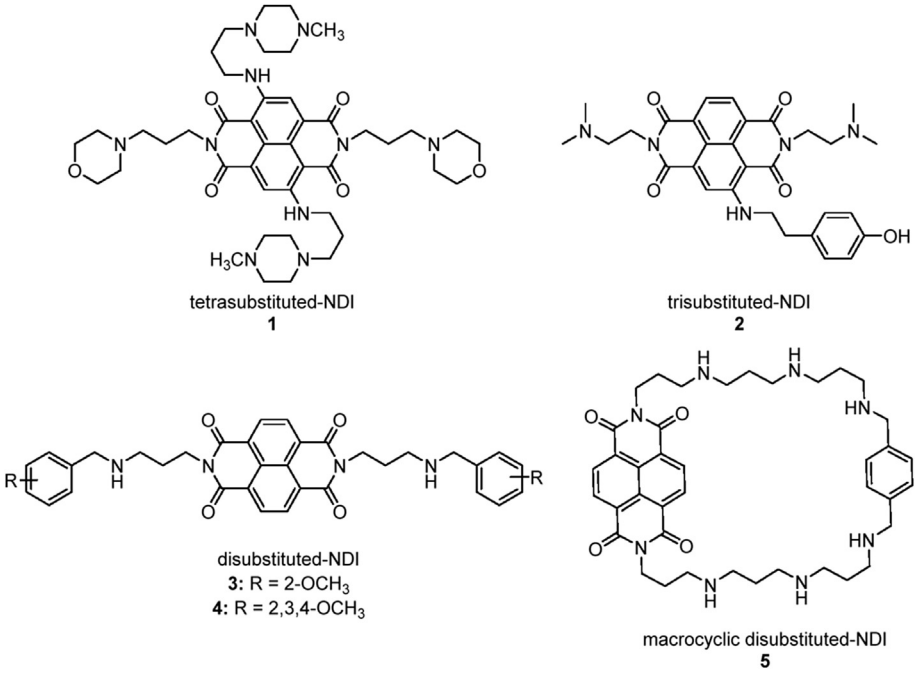

Fig. 1. Selected NDI-based G-quadruplex binders reported in literature.

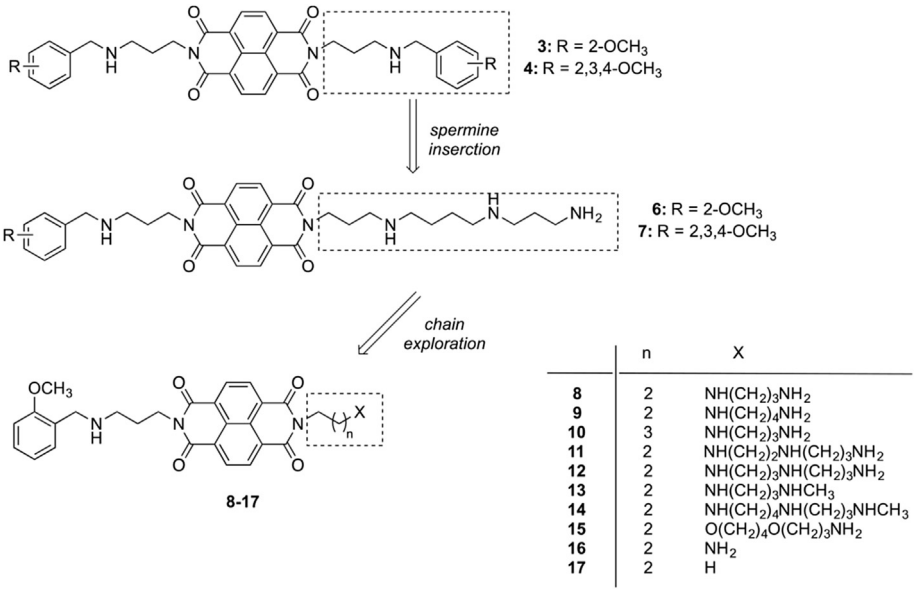

	n	X
8	2	$NH(CH_2)_3NH_2$
9	2	$NH(CH_2)_4NH_2$
10	3	$NH(CH_2)_3NH_2$
11	2	$NH(CH_2)_2NH(CH_2)_3NH_2$
12	2	$NH(CH_2)_3NH(CH_2)_3NH_2$
13	2	$NH(CH_2)_3NHCH_3$
14	2	$NH(CH_2)_4NH(CH_2)_3NHCH_3$
15	2	$O(CH_2)_4O(CH_2)_3NH_2$
16	2	NH_2
17	2	H

Fig. 2. Drug design leading to compounds **6**–**17.**

by a spermidine-like chain (**8**, 3-3; **9**, 3–4; **10**, 4–3); *ii*) **11** and **12** characterized by a spermine-like chain (**11**, 3-2-3; **12**, 3-3-3); *iii*), **13** and **14** are the *N*-methyl derivatives of **8** and **6**, respectively, *iv*) **15** deriving from the substitution with oxygens of the inner nitrogen atoms of the spermine portions of **6**; *v*) **16** bearing only one amine function and **17** carrying an uncharged ethyl group in the lateral chain.

2. Results and discussion

2.1. Chemistry

Synthesis of the intermediates and target compounds have been performed following the procedure depicted in Schemes 1–3. Boc-protected (poly) amines **18**–**22** have been obtained through the standard procedure reported in literature [24]. Boc-protected polyamines **31** and **32** have been synthesized as reported in Scheme 1. 3-amino-1-propanol or 4-amino-1-butanol have been protected as trifluoroacetamide (**23** and **24**) and then activated at the hydroxyl group as tosylate leading to **25** and **26**. Reaction of the tosylates with monoBoc-diaminopropane **27** or monoBoc-diaminobutane **28** has led to the protected triamine **29** and **30**, respectively. In situ Boc-protection of the secondary nitrogen atom of **29** and **30** and then trifluoroacetamide deprotection provided diBoc-protected triamines **31** and **32**, respectively. *N*-methyl mono-Boc triamine **43** and *N*-methyl di-Boc tetraamine **44** have been synthesized as reported in Scheme 2. Protection of the inner nitrogen atom(s) of spermidine and spermine following standard procedures has led to monoBoc-triamine **33** and diBoc-tetraamine **34**. Then, **33** and **34** have been selectively benzylated at only one of the primary amine function through reaction with benzaldehyde and *in situ* reduction with $NaBH_4$ of the formed Schiff base gave **35** and **36**, respectively. The free primary amino groups of **35** and **36** have been protected as trifuoroacetamide to give **37** and **38**. The secondary amino groups have been subjected to mono-alkylation with methyl iodide to give **39** and **40** that, after deprotection of the primary amino group gave **41** and **42**, respectively. Subsequent debenzylation of those intermediates with H_2/Pd furnished **43** and **44**. Compounds **49**–**59** and **17** have been obtained refluxing a stoichiometric mixture of naphtalentetracarboxylic dianhydride, 2-methoxybenzylpropylendiamine **45** or 2,3,4-trimethoxybenzylpropylendiamine **46** and the Boc-protected amines **18**–**22**, **31**, **32**, **43**, **44**, **47** and amine **48** in DMF (Scheme 3). Acidic hydrolysis of intermediates **49**–**59** has finally led to the desired products **6**–**16** as hydrochloride salts.

2.2. Biochemical and biophysical studies

Target compounds **6**–**17** have been firstly evaluated for their ability to stabilize hTel G-quadruplex and dsDNA sequences. Compound **3** has been used as reference compound. Fluorescence melting experiments were performed in the 0–20 μM compound

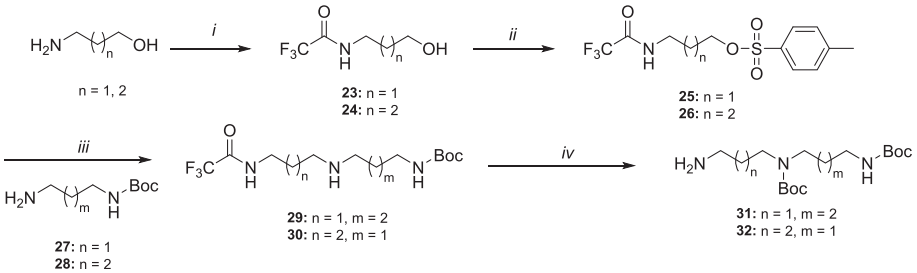

Scheme 1. *i)* CF_3COOEt, rt, 1 h, quantitative yields; *ii)* tosylchloride, Et_3N, DMAP, CH_2Cl_2, rt, overnight, 55–60% yields; *iii)* THF, rt, overnight, 35–47% yields; *iv)* a. Boc_2O, Methanol, rt, 16 h; b. NaOH 40%, Methanol, rt, 16 h, 64–87% yields.

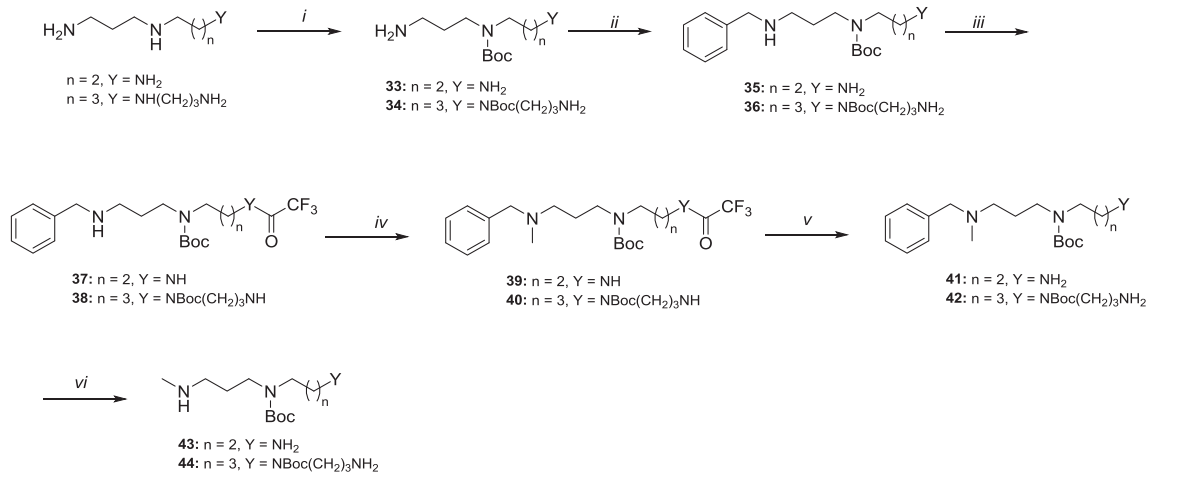

Scheme 2. *i)* a. CF_3COOEt, Methanol, −78 °C, 16 h; b. Boc_2O, DCM, rt, 12 h; c. NaOH 40%, Methanol, rt, 12 h, 45–56% yields; *ii)* a. benzaldehyde, Methanol, reflux, 5 h, b. $NaBH_4$, EtOH, rt, 16 h, 80–91% yield; *iii)* CF_3COOEt, Et_3N, rt, 16 h, 72–92% yield; *iv)* CH_3I, Et_3N, THF, rt, 24 h, 30–66% yield; *v)* NaOH 40%, Methanol, rt, 16 h, 88–92% yields; *vi)* H_2/Pd, Methanol, rt, 5 h, 68–76% yields.

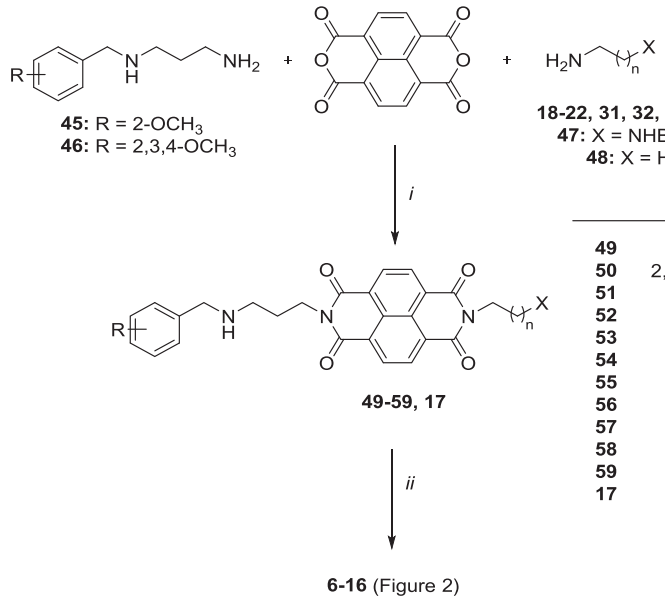

	R	n	X
49	2-OCH_3	2	$NBoc(CH_2)_4NBoc(CH_2)_3NHBoc$
50	2,3,4-OCH_3	2	$NBoc(CH_2)_4NBoc(CH_2)_3NHBoc$
51	2-OCH_3	2	$NBoc(CH_2)_3NHBoc$
52	2-OCH_3	2	$NBoc(CH_2)_4NHBoc$
53	2-OCH_3	3	$NBoc(CH_2)_3NHBoc$
54	2-OCH_3	2	$NBoc(CH_2)_2NBoc(CH_2)_3NHBoc$
55	2-OCH_3	2	$NBoc(CH_2)_3NBoc(CH_2)_3NHBoc$
56	2-OCH_3	2	$NBoc(CH_2)_3NHCH_3$
57	2-OCH_3	2	$NBoc(CH_2)_4NH(CH_2)_3NHCH_3$
58	2-OCH_3	2	$O(CH_2)_4O(CH_2)_3NHBoc$
59	2-OCH_3	2	NHBoc
17	2-OCH_3	2	H

Scheme 3. *i)* DMF, reflux, 5 h, 15–30% yields; *ii)* HCl 6 N, rt, overnight, quantitative yields.

concentration range: the increment of the melting temperatures of the nucleic acid induced by all tested ligands at 2.5 μM is reported in Table 1. As already introduced, compounds **6** and **7**, deriving from compounds **3** and **4**, respectively, were initially synthesized and analysed to establish the more suitable substituent on the aromatic ring for the G-quadruplex recognition: they share the same spermine chain on one side of the NDI scaffold and differ for the number of the methoxy groups on the terminal aromatic ring. From Table 1, compound **6** emerges as a better G-quadruplex binder than compound **7** (**6**, ΔTm = 21.4 °C *vs* **7**, ΔTm = 13.1 °C at 2.5 μM) highlighting that, in these NDI-spermine derivatives, the 2,3,4-mehoxybenzyl group has an unfavourable effect on the G-quadruplex stabilization. Further, compound **7** is a better dsDNA binder (**6**, ΔTm = 6.7 °C *vs* **7**, ΔTm = 12.6 °C). These results are surprising in light of the previously reported data on symmetric derivatives, where compound **4** proved to be a better G-quadruplex binder than compound **3,** suggesting a possible different binding mode towards target DNA for the new polyamine conjugates **6** and **7** [20].

Closely related to compound **6**, compounds **11** and **12** are characterized by shorter spermine-like side chains differing in the number of methylene groups separating the inner nitrogen atoms. In this series, the decrease of the methylene groups from four to three, such as in compound **12**, induces a slight decrement in the stabilization of telomeric G-quadruplex (ΔTm = 16.3 °C) while the lower homologue **11**, characterized by a 3-2-3 chain, has a stabilization capacity comparable to compound **6** (ΔTm = 22.0 °C). Among derivatives **8**–**10** that contain shorter spermidine-like chain, compound **9** (3–4) emerges as the most effective G-quadruplex binder with a ΔTm value of 29 °C at 2.5 μM, significantly higher than the one displayed by compound **6**. This result was unexpected since we have previously reported that the elimination of amine functions is usually accompanied with a concomitant decrease of the quadruplex stabilizing capacity [16]. The related derivative **8** preserves good DNA binder activity whereas compound **10** shows a significantly impaired ability to stabilize the telomeric G-quadruplex being the weaker G-quadruplex binder

Table 1
Effects of compounds **3**, **6**–**17** on the thermal stability of hTel G-quadruplex and dsDNA and on the catalytic activity of topoisomerase IIα and TAQ polymerase.

Compound	ΔTm (°C)[a]		ΔΔTm[b]	Topoisomerase IIα IC_{50} (μM)[c]	TAQ Polymerase MIC (μM)[d]
	hTel G-quadruplex	dsDNA			
3	20.5	8.4	12.1	6.0 ± 0.9	10 ± 2
6	21.4	6.7	14.7	2.2 ± 0.4	0.25 ± 0.06
7	13.1	12.6	0.5	n.d.[e]	n.d.[e]
8	13.3	7	6.3	1.5 ± 0.2	0.25 ± 0.06
9	29	12.2	16.8	8.1 ± 1.1	0.5 ± 0.1
10	22.2	9.1	13.1	7.0 ± 0.5	0.5 ± 0.1
11	22	10.4	11.6	n.d.[e]	n.d.[e]
12	16.3	12.2	4.1	n.d.[e]	n.d.[e]
13	18	9.5	8.5	n.d.[e]	n.d.[e]
14	26.1	17.1	9.0	n.d.[e]	n.d.[e]
15	12.9	1.5	11.4	5.5 ± 0.5	1.0 ± 0.2
16	1.4	6.7	−5.3	n.d.[e]	n.d.[e]
17	2.4	0.9	1.5	n.d.[e]	n.d.[e]

[a] Increment of the melting temperature induced by 2.5 μM ligand concentration. Errors were ±0.4 °C.
[b] ΔΔTm was derived as the difference of the thermal stabilization of the two DNA substrates.
[c] IC_{50} values are defined as the drug concentration which reduces by 50% the activity.
[d] MIC as the minimal drug concentration at which the enzymatic activity is suppressed.
[e] n.d. = not determined.

within the spermidine-like series with a ΔTm value of 13.1 °C at 2.5 μM.

Compounds **13** (3-3-CH_3) and **14** (3-4-3-CH_3) were synthesized in order to evaluate the effect of the alkylation of the primary amine function of polyamine chain of compounds **8** and **6**, respectively. Both compounds display improved G-quadruplex binding profiles compared to the parent compounds (**13** *vs* **8** and **14** *vs* **6**); unfortunately, for compound **14** a larger increase of the affinity towards dsDNA is observed (dsDNA: **6**, ΔTm = 6.7 °C at 2.5 μM; **14**, ΔTm = 17.1 °C at 2.5 μM) thus leading to a reduced selectivity. Replacement of the inner nitrogen atoms of **6** with oxygens (as in compound **15**) induces a marked reduction of the G-quadruplex DNA-binding activity (ΔTm = 12.9 °C at 2.5 μM) underlying that the establishment of interaction between the secondary amine function of the polyamine side chain and DNA is involved in stabilizing the G-quadruplex arrangements. This was further confirmed by the worst G-quadruplex affinities of compound **16**, carrying only one amino group, and compound **17** where the polyamine has been replaced by an alkyl chain.

To better highlight the potential selectivity towards G-quadruplex structure, we compared the thermal stabilization on the two DNA templates in terms of ΔΔTm ($\Delta Tm_{G\text{-}quadruplex}$- ΔTm_{dsDNA}) (Table 1). From this analysis, compounds **9** and **6** emerged as the most selective ones. This suggested that they conserved spacer's length in the polyamine chain that is beneficial for the recognition of the telomeric G-quadruplex. At the same time, it indicated that the presence of an additional basic functionality, such as in compound **6**, did not increase the interaction with the nucleic acid neither in terms of efficiency and selectivity (see **6** *vs* **9** and **12** *vs* **8**).

Compound **15** showed a good preference towards G-quadruplex but, as above discussed, this is counterbalanced by a reduced affinity on both templates as a result of the substitution of two nitrogen atoms with oxygen atoms in the lateral chain.

These data indicated that some of the new derivatives were more promising G-quadruplex binders in comparison to the lead compound **3**. However, in no instance we succeed to realize a total suppression of the dsDNA recognition thus letting open the maintenance of a multiple target mechanism of actions. Based on these observations, we selected the most promising G-quadruplex binders **6** and **9**, together with their homologues **8** and **10**, and **15** to explore the functional role of the basic amine functions in the side chain on the activity of DNA processing enzymes, such as topoisomerase IIα and TAQ-polymerase. We first assessed the interference of our ligands on topoisomerase IIα activity (Fig. 3A). It resulted that the tested derivatives inhibit the enzyme with comparable efficiency to the lead compound **3** with the notable exception of **8** and **6** for which significantly reduced IC_{50} values were detected (IC_{50} of 1.5 and 2.2 μM, respectively) (Table 1). It is well known that compounds active against topoisomerases may work as protein inhibitors or poisons (stabilizers of protein-DNA cleavage complex). By a cleavage assay, we confirmed that none of the tested compounds was able to stabilize the cleavage complex topoisomerase-DNA (Fig. 3B), thus ruling out poisoning as mechanism of action.

To further validate this model, we explored the effect of the tested derivatives on the activity of an additional DNA processing enzyme, TAQ-polymerase (Fig. 3C, Table 1). Consistently, derivatives **8** and **6** resulted the most active also against TAQ-polymerase, with a complete suppression of enzyme activity at 0.25 μM. Interestingly, the ranking order obtained for topoisomerase II inhibition was essentially conserved among asymmetric derivatives but with an efficiency significantly higher with reference to the symmetrically substituted control **3** (10 ± 2 μM).

This suggested that within asymmetric derivatives, the inhibition of the two studied protein targets, topoisomerase IIα and TAQ-polymerase, is probably related to DNA/ligand interaction rather than to a ligand/protein interaction. In this model, the more pronounced efficiency of derivatives **6** and **8** might underline a modulation of the binding mode. This point was supported by agarose gel electrophoresis of supercoiled plasmid treated with **8**–**10** (Fig. 3D). The bell-shaped reduction of the DNA electrophoretic mobility induced by tested derivatives indicates that **9** intercalates within the dsDNA starting from higher concentration in comparison to **8**, which, on turn, causes a significant precipitation of the nucleic acid at the highest tested concentrations. Conversely, **10** binds plasmid DNA as evidenced by the smear of the plasmid electrophoretic band, but without evidence of intercalation.

Thermal analysis underlined that selected compounds bind both the ds and the telomeric G-quadruplex DNAs. Finally, we investigated if the detected stabilization of the G-quadruplex form of telomeres exerted by the selected NDI derivatives can interfere with telomerase activity. However, working at ligands concentrations that are no affecting TAQ-polymerase activity, no specific inhibition of telomerase by the selected compounds was observed,

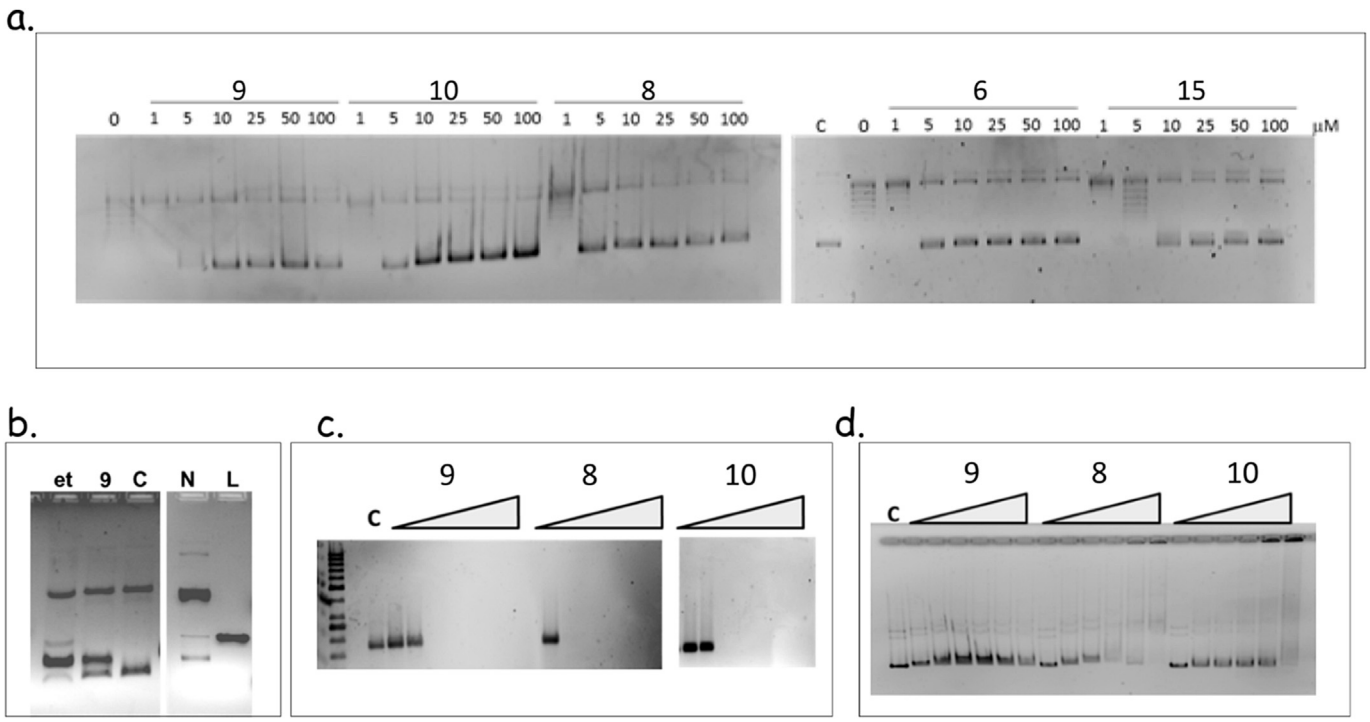

Fig. 3. a) Inhibition of the relaxation of supercoiled pBR322 promoted by 1 U of IIα due to addition of increasing concentrations compounds **6**, **8**–**10**, 15 in the reaction mixture; b) Cleavage assay performed on pBR322 with 5 U of topoisomerase IIα (lane C) in the presence of Etoposide (lane et) or compound **9** (lane **9**). Lanes N and L refer to the nicked and linearized pBR322, respectively; c) Inhibition of the amplification of a fragment of pBR322 mediated by TAQ polymerase chain reactions performed in the presence of increasing concentrations of compounds **8**–**10** (0.25–0.5-1.0-2.5-5.0-10-20-40 μM); d) Modification of the electrophoretic mobility of supercoiled pBR322 upon addition of compounds **8**–**10** (0–100 μM) in 10 mM Tris, 50 mM KCl, in the absence of any enzyme.

thus ruling out this mechanism as the preferential one. This is not surprising since we and others have already reported that NDIs highly effective in stabilizing telomeric G-quadruplex are not able to inhibit telomerase *in vitro* or in cells [16,25].

2.3. Molecular modelling studies

Compounds **9**, **11** and the worst binder **16** were submitted to a conformational search with the Monte Carlo method (MC) coupled to the analysis of the Solvent Accessible Surface Area (SASA) computed onto a defined NDI planar aromatic system. Among all the generated conformations, those within 3 kcal/mol above the energy global minimum were selected and submitted to the Boltzmann Accessible Solvent Accessible Surface Area (BASASA) analysis [26] (Table S1) (*see Materials and Methods*), while the conformer with the lowest potential energy (Table S2) has been submitted to docking calculations. In addition, to take into account the G-quadruplex DNA and dsDNA flexibility, a 10 ns long Molecular Dynamics (MD) simulation has been carried out as described in the Material and Methods section. The geometrical stability of the G-quadruplex DNA hybrid-1 and hybrid-2 forms is demonstrated by their RMSD average calculated for the all heavy atoms of the nucleic acid (3.22 ± 0.15 Å and 2.69 ± 0.14 Å, respectively) (Fig. S2A) and the G-tetrads atoms only (1.09 ± 0.08 Å and 1.07 ± 0.09 Å, respectively) (Fig. S2B). MD trajectories were then clustered using the GROMOS algorithm [27] of the g-cluster tool implemented in GROMACS ver. 4.5 [28]. Three main clusters were found both from hybrid-1 (PDB code: 2JSM) [29] (Fig. S3A) and hybrid-2 (PDB code: 2JSL) [29] (Fig. S3B) MD trajectories, but only the one most different has been taken into account for docking simulations (Table S3).

2.3.1. Binding mode of compounds 9, 11 and 16 against G-quadruplex/ds DNAs

To get further insight into the binding mode and clarify the role of the spermine and spermidine-like side chains in the DNA recognition of the NDI derivatives **9**, **11** and **16**, molecular docking calculations have been performed with AutoDock4.2 [30] and a ligand/G-quadruplex DNA stoichiometry ratio of 2:1 has been considered to respect the experimental findings. All the 100 binding poses predicted by AutoDock4.2 were then submitted to a full energy optimization step using the AMBER* force field as implemented in MacroModel ver. 10.8 [31]. The same protocol has been adopted also against the homology model of the experimental sequence of the dsDNA, considering a 1:1 stoichiometry ratio.

2.3.1.1. Hybrid-1. A geometrical analysis of the binding poses between spermidine-like NDI **9** and spermine-like NDI **11** against the hybrid-1 G-quadruplex DNA (Fig. 4A and B respectively) reveals a groove recognition of compounds **9** and **11**, probably also due to the steric hindrance of the residues T18:A1:A19 at the 5′ and T23:T12:T11:A13 at the 3′, which stacks at the center of the top and bottom G-tetrad planes thus hampering the π-π stacking of the NDI core. Specifically, in the 2:1 complex of compound **9** (Fig. 4A) the spermidine-like side chain and the NDI core globally engage eight hydrogen bonds (H-bonds) with the phosphate groups of G2:G22:G4 and G20:G15:G14, while globally five electrostatic interactions are established between two positively charged nitrogen atoms and the phosphate backbone of G4:G2:G14:G15:G16 residues. The NDI is involved also in four T-shaped π-π stacking with G3:G22:G2:G21 and G14:G15:G16 residues. As concern the molecular recognition of compound **11** (Fig. 4B), the three methylene linker of the spermine chain globally engages eight H-bonds with the phosphate groups of G21:G22:G10:T11:G10 and six

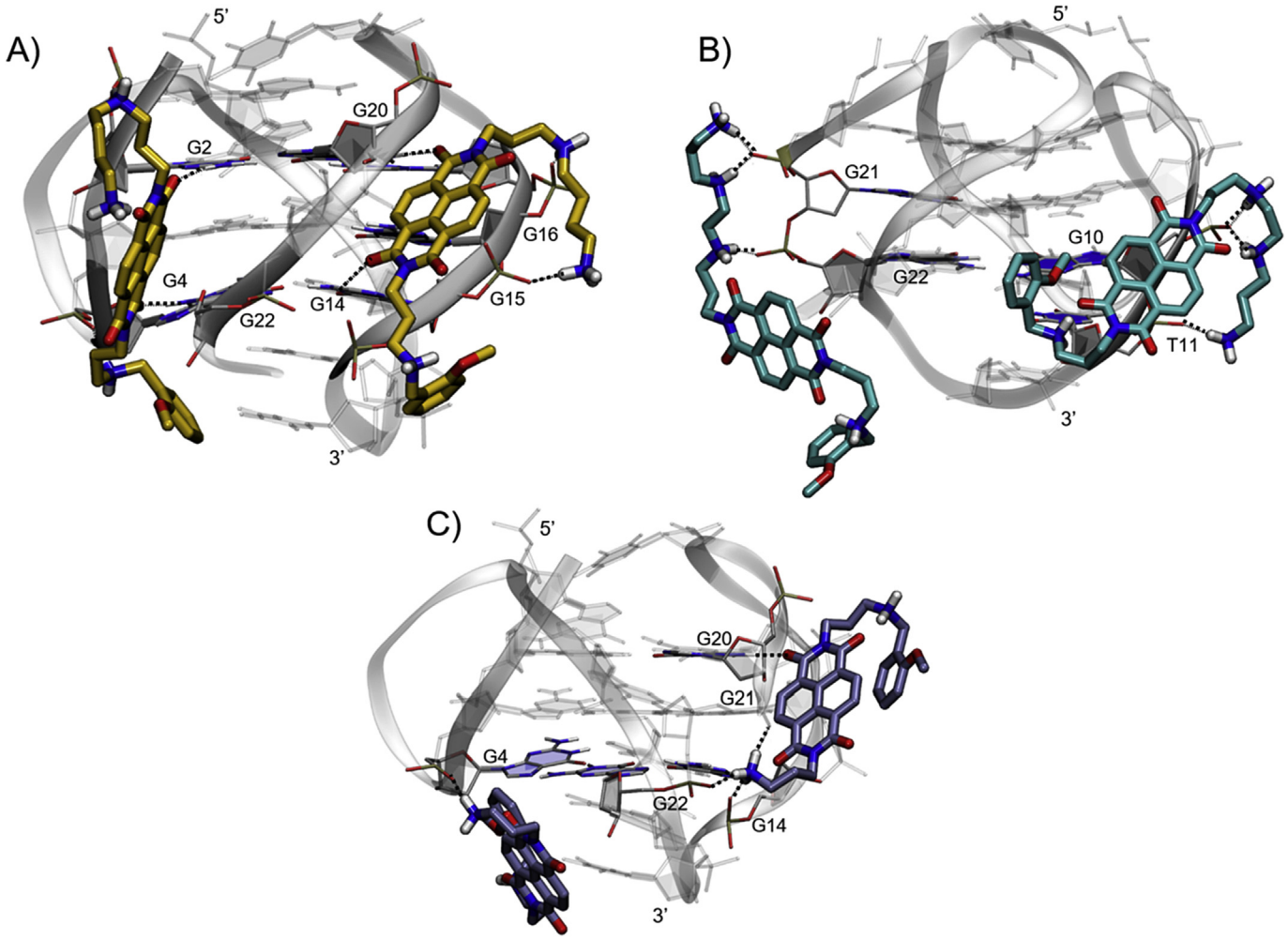

Fig. 4. 2:1 binding mode against the hybrid-1 form of G-quadruplex DNA receptor (PDB code: 2JSM) of the NDI polyamine derivatives (**A**) **9**, (**B**) **11** and the worst binder (**C**) **16**. Nucleic acid is displayed as grey ribbon while interacting residues as stick coloured by atom type. Polyamine NDIs **9**, **11** and **16** are shown as yellow, cyan and iceblue sticks respectively. (For interpretation of the references to colour in this figure legend, the reader is referred to the web version of this article.)

electrostatic interactions with T11:T12:G10:G15:G21:G22. Only one T-shaped π-π stacking is established, instead, between the 2-methoxybenzyl group and T23. The role of the spermidine-like and spermine side chains in G-quadruplex DNA recognition is better highlighted comparing the binding mode of compounds **9** and **11** with that of the worst binder **16**, which bears only one ionized nitrogen atom without any polyamine chain. The absence of spermidine or spermine side chains reduces the number of H-bonds rather than the electrostatic interactions. Compound **16** engages, in fact, five H-bonds and five electrostatic interactions with the terminal positively charged nitrogen atom of the three methylene side chain and the phosphate groups of G4:G20:G22:G14:G21.

2.3.1.2. Hybrid-2. Similarly to hybrid-1, also the binding mode against hybrid-2 conformation (PDB code: 2JSL) (Fig. 5) is characterized by a groove recognition, since the steric hindrance of T11:T12:A13:A1 and T23:A7:T6 at the 5'-end and the 3'-end respectively, hinders the π-π stacking with the NDI core. With respect to the hybrid-1 topology, the molecular recognition of compound **9** towards hybrid-2 is characterized by a slightly lower number of both H-bonds and electrostatic interactions of the spermidine side chain that is more solvent exposed (Fig. 5A). Seven H-bonds and four electrostatic interactions are engaged, in fact, with residues G22:G4:G14:G15:G16 and the phosphate backbone of G4:G8:G15:G16, respectively. A lower number of electrostatic interactions are observed also for compound **11**. In this case, in fact, the spermine-like side chain of compound **11** is globally involved in ten H-bonds with the phosphate backbone of G2:G4:G22:G4:T18:G16:T17 residues and only four electrostatic interactions with G2:G4:T18:T17 (Fig. 5A). In addition, the 2-methoxybenzyl group of compound **11** is involved in three T-shaped π-π stacking with G14:G14. The reduced number of electrostatic interactions that occurs in the hybrid-2 topology for both compounds **9** and **11** could be attributed to an increased water solvent exposure of both spermidine and spermine-like side chains with respect to the hybrid-1 topology.

2.3.1.3. ds-DNA. Concerning the dsDNA recognition of compounds **9**, **11** and **16**, despite the presence of an intercalative binding site, the most populated clusters found the major and the minor grooves as the most involved binding sites in the recognition of the NDIs polyamine (Fig. S4) with both spermidine and spermine-like side chains of compounds **9** and **11** involved in a much lower number of H-bonds and electrostatic interactions with the phosphate backbone with respect to G-quadruplex DNA (Fig. S4A).

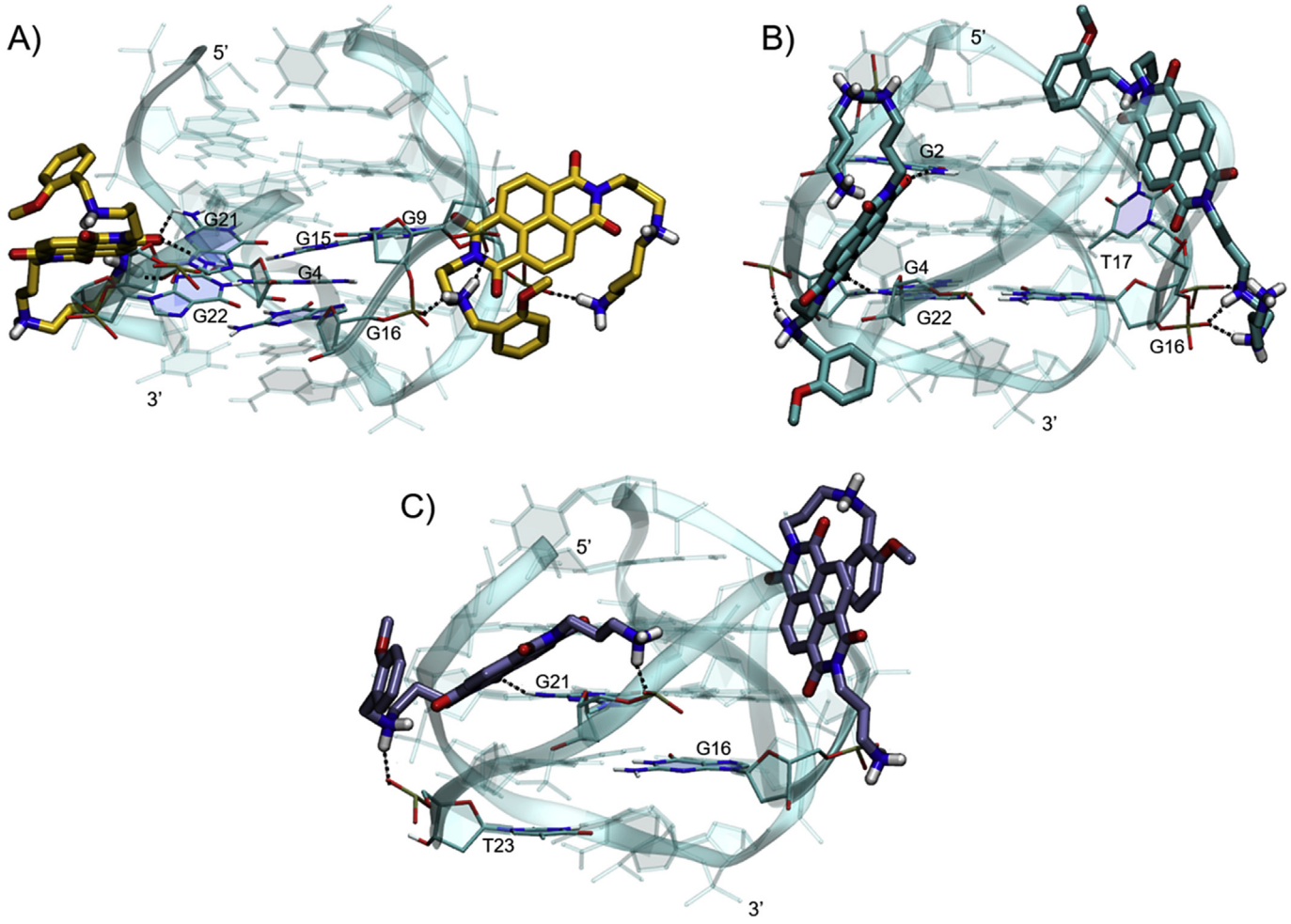

Fig. 5. 2:1 binding mode against the hybrid-2 form of G-quadruplex DNA receptor (PDB code: 2JSL) of the NDI polyamine derivatives (**A**) **9**, (**B**) **11** and the worst binder (**C**) **16**. Nucleic acid is displayed as light-cyan ribbon while interacting residues as stick coloured by atom type. Polyamine NDIs **9**, **11** and **16** are shown as yellow, cyan and iceblue sticks respectively. (For interpretation of the references to colour in this figure legend, the reader is referred to the web version of this article.)

2.4. Antiproliferative and proapoptotic activities

All the synthesized compounds were evaluated for antiproliferative activity in the National Cancer Institute's 60 cell lines screen. Compounds **6**, **8**–**11**, **13**–**17** were selected for screening at five concentrations using 10-fold dilutions ($10^{-4} - 10^{-8}$ M) on the full panel of approximately 60 human cancer cell lines derived from 9 human cancer cell types that have been grouped into disease subpanels including leukemia, non-small cell lung, colon, central nervous system, melanoma, ovarian, renal, prostate, and breast tumor cell lines (Table 2 and Table S4). The antiproliferative activity of the compounds was given as GI_{50} (the molar concentration of the compound that inhibits 50% net cell growth). An evaluation of the data reported pointed out that all the tested compounds exhibit antiproliferative activity against all the human cell lines in the micro to sub-micromolar range of concentration. In general, compounds characterized by a spermidine-like side chain, such as compounds **8** and **9**, show the best GI_{50} values. The most active compound of the series (with the exception of some cell lines) is compound **9,** which is characterized by the higher value of ΔTm towards G-quadruplex. Compound **9** does not show any particular cell line selectivity being active in the sub-micromolar range of concentration in all the cell lines assayed. The most sensitive cell lines are SR (leukemic) with a GI_{50} value of 78 nM and MDA-MB-468 (breast cancer) with a GI_{50} value of 85 nM. The less sensitive cell line is UO-31 (renal cancer) characterized by a GI_{50} value of 1.86 μM. Compound **8** is the most active compound in some lines: in particular, in OVCAR-8 it is an order of magnitude more active than compound **9**. Compound **10**, characterized by a 4-3 chain, is, in general, less active than **8** and **9** displaying also the worst GI_{50} value of all the series towards SNB-75 (CNS cancer) cell line (GI_{50} = 16.74 μM). Compound **6**, carrying a spermine chain, although being less active than compound **9**, is characterized by a good level of antiproliferative activity. At the opposite, its homologue **11** shows the less promising activity in some cell lines (*i.e.* GI_{50} = 10.8 μM in UO31 cell line). Methylation of the terminal nitrogen atom has a detrimental effect on the growth inhibition activity (**6** *vs* **14**). In particular, despite its good ΔTm value, compound **14** is the less active compound of the series in most of the cell lines. Surprisingly, reduction of the number of nitrogen atoms or their replacement with oxygens does not have a detrimental effect as high as observed with compound **14**.

Next, the ability of compounds **8** and **9** to induce apoptotic cell death was evaluated. Compound **8** induced a significant increase in apoptotic events only at the highest concentration used (14.5% *vs* 6.6% of untreated cells) while compound **9** showed 17.9% of apoptotic cells at 3.2 μM and 22.2% at 6.4 μM *vs* 5.8% of untreated cells (Fig. 6A).

Table 2
Overview of the *in vitro* antiproliferative screening results for compounds **6**, **8**–**11**, **13**–**17**.

cpd	MG_MID[a] (GI_{50}[b], μM)	Cell lines (GI_{50}[b], μM)		cpd	MG_MID[a] (GI_{50}[b], μM)	Cell lines (GI_{50}[b], μM)	
		Most sensitive	Less sensitive			Most sensitive	Less sensitive
6	0.680	breast MDA-MB 468 (0.133)	renal UO-31 (2.675)	**13**	1.61	leukemia SR (0.270)	renal UO-31 (5.88)
8	0.621	leukemia SR (0.028)	renal TK-10 (1.61)	**14**	3.02	breast T47-D (0.342)	NSCL NCI-—H522 (5.62)
9	0.360	leukemia SR (0.076)	renal UO-31 (1.86)	**15**	1.10	ovarian OVCAR-4 (0.197)	NSCL HOP-62 (2.66)
10	2.18	leukemia SR (0.038)	renal CAKI-I (13.15)	**16**	1.19	leukemia SR (0.167)	ovarian ADR-RES (2.90)
11	3.65	leukemia MOLT-4 (0.173)	renal CAKI-I (21.7)	**17**	0.95	ovarian OVCAR-4 (0.152)	NSCL HOP-92 (2.654)

[a] MG_MID = mean graph midpoint: arithmetic mean value for all tested cancer cell lines.
[b] GI_{50} = concentration (μM) that inhibits 50% net cell growth.

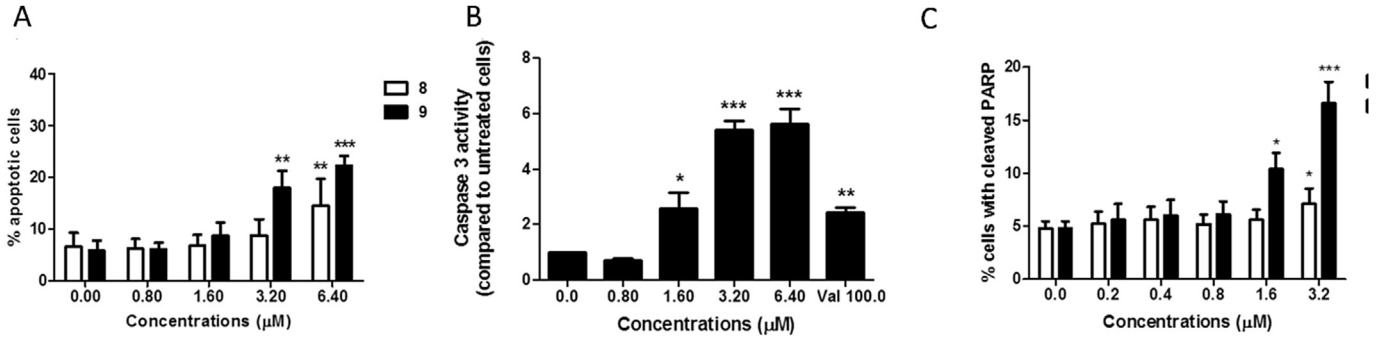

Fig. 6. A) Apoptotic cells after 24 h treatment with compounds **8** or **9**. **P < 0.01; ***P < 0.001. B) Caspase-3 activity of Jurkat cells after 24 h treatment with compound **9** or 1 h with valinomycin (Val). *P < 0.05; **P < 0.01; ***P < 0.001. C) Fraction of Jurkat cells with cleaved PARP after 24 h treatment with compounds **8** or **9**. *P < 0.05; ***P < 0.001.

Moreover, the activation of caspase-3 was evaluated. This enzyme showed an enhanced activity: a 2.6-fold increase was observed in cells treated with compound **9** at 1.6 μM and a 5.6-fold increase at 6.4 μM (Fig. 6B).

The activation of caspase-3 was further confirmed by poly(ADP) ribose polymerase (PARP) cleavage in Jurkat cells. PARP, an enzyme important in genome surveillance, is one of the natural substrates cleaved by caspases during apoptosis. PARP is an important reporter of caspase-3 activation and both compounds **8** and **9** induced PARP cleavage starting from the concentration of 3.2 μM. However, their proapoptotic potential was different: compound **8** showed a slight increase (7.2%) of cells with cleaved PARP compared to compound **9** that induced 16.6% of cells with cleaved PARP *versus* 4.8% of untreated cells (Fig. 6C).

Both compounds **8** and **9** significantly altered cell-cycle residence. At 3.2 μM, compound **8** caused an accumulation of cells in the G2/M phase (27.8% *vs* 20.8% of untreated cells) accompanied by a slight compensatory decrease of cells in the G0/G1 phase (56.1% *vs* 62.7% of untreated cultures) (Fig. 7A). Similarly, compound **9**, at the same treatment concentration (3.2 μM), induced an accumulation of cells in the G2/M phase (20.8% *vs* 17.1% of untreated cells) and a decrease of cells in the G0/G1 phase (59.7% *vs* 68.6% of control) (Fig. 7B).

3. Conclusion

In summary, with the aim of expanding the structure-activity relationship studies of compound **3** and to obtain compounds endowed with increased antiproliferative activity, a series of hybrid NDI-polyamines **6**–**17** has been synthesized. The replacement of a 2-methoxybenzylpropylendiamine group of compound **3** with a spermidine chain has a positive effect in the G-quadruplex recognition process, as compound **9** is more active than the parent compound. Furthermore, this substitution has a positive effect also concerning the selectivity, since compound **9** is characterized by a lower affinity than compound **3** to non-quadruplex DNA, and the inhibitory activity toward other anticancer targets, such as topoisomerase IIα and *TAQ* -polymerase. Compound **9** exhibits high antiproliferative activity against about 60 human tumor cell lines with GI_{50} values reaching nanomolar concentrations in leukemia and breast cancer cell lines (i.e. SR and MDA-MB-468). The high level of *in vitro* and cellular activities suggest that compound **9** may represent a promising hit for the development of new antiproliferative agents. Furthermore, the binding mode of the most interesting compounds **9** and **11** against G-quadruplex and dsDNAs has been elucidated, confirming the importance of the spermidine and spermine side chains in engaging H-bond and electrostatic interactions with the phosphate backbone of the G-quadruplex

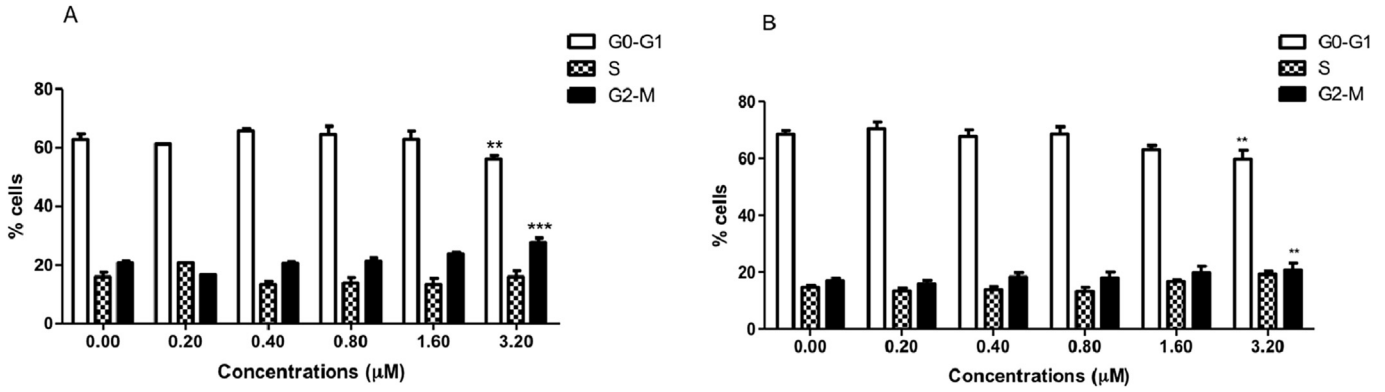

Fig. 7. Cell-cycle distribution of Jurkat cells following 24 h of treatment with compounds **8** (A) or **9** (B). **P < 0.01; ***P < 0.001.

DNA, particularly with the hybrid-1 topology. Overall, in the hybrid-2 form, in fact, a reduced number of electrostatic interactions has been observed both for **9** and **11,** probably due to a greater water solvent exposure of the spermidine and spermine side chains. Surprisingly, the major and the minor groove of the dsDNA are the binding site mainly involved in the molecular recognition.

4. Experimental section

4.1. Chemistry

4.1.1. General information

Uncorrected melting point was taken in glass capillary tubes on a Buchi SMP-20 apparatus. The elemental analysis was performed with Perkin Elmer elemental analyzer 2400 CHNESI. MS spectra were recorded on Perkin Elmer 297 and Waters ZQ 4000 and Micromass Q-TOF Ultima Global. ^{1}H NMR and ^{13}C NMR were recorded on Varian VRX 200 and 400 instruments. Chemical shifts are reported in parts per million (ppm) relative to peak of tetramethylsilane (TMS) and spin multiplicities are given as s (singlet), br s (broad singlet), d (doublet), t (triplet), q (quartet) or m (multiplet). Chromatographic separations were performed on silica gel columns by flash (Kieselgel 40, 0.040 e 0.063 mm, Merck) column chromatography. Reactions were followed by thin layer chromatography (TLC) on Merck (0.25 mm) glass-packed precoated silica gel plates (60 F254) and then visualized in an iodine chamber or with a UV lamp.

*4.1.2. General procedure for the synthesis of **23** and **24***

To a cooled solution (0 °C) of the appropriate aminoalcohol (1 eq) was added dropwise ethyltrifluoroacetate (1.2 eq) and the resulting mixture was stirred at room temperature of 2 h. The solvent was evaporated in vacuum and the product obtained was used without further purification.

*4.1.2.1. 2,2,2-Trifluoro-N-(3-hydroxypropyl)acetamide **(23)**.* Yellow oil, quantitative yield; ^{1}H NMR (400 MHz, $CDCl_3$) δ 1.70–1.78 (m, 2H), 3.18 (t, 2H, J = 5.1 Hz), 3.69 (brs, 1H, exch D_2O), 3.52 (t, 2H, J = 4.8 Hz), 8.74 (brs, 1H, exch D_2O); ^{13}C NMR (100 MHz, $CDCl_3$) δ 30.5, 38.4, 61.0, 115.9, 157.8; HMRS (esi) m/z calcd for $C_5H_9F_3NO_2$ [M+H] 172.0585, found 172.0576.

*4.1.2.2. 2,2,2-Trifluoro-N-(4-hydroxybutyl)acetamide **(24)**.* Yellow oil, quantitative yield; ^{1}H NMR (300 MHz, $CDCl_3$) δ 1.53–1.66 (m, 4H), 3.31 (t, 2H, J = 10.0 Hz), 3.65 (t, 2H, J = 7.2 Hz), 3.79 (brs, 1H, exch D_2O), 8.02 (brs, 1H, exch D_2O); ^{13}C NMR (100 MHz, $CDCl_3$) δ 26.8, 29.9, 39.4, 62.3, 115.6, 157.8; HMRS (esi) m/z calcd for $C_6H_{11}F_3NO_2$ [M+H] 186.0742, found 186.0569.

*4.1.3. General procedure for the synthesis of **25** and **26***

Et_3N (2 eq), tosyl chloride (1.2 eq) and a catalytic amount of DMAP were added to a cooled solution of **23** or **24**, respectively (1 eq) in DCM and the resulting mixture was stirred at room temperature for 16 h. Removal of the dried solvent gave a residue that was purified by flash chromatography using as eluent a mixture of ethyl acetate/petroleum ether (6:3), providing the desired products **25** and **26**.

*4.1.3.1. 3-(2,2,2-trifluoroacetamido)propyl 4-methylbenzenesulfonate **(25)**.* Yellow solid, 55% yield; ^{1}H NMR (400 MHz, $CDCl_3$) δ 1.94–2.00 (m, 2H), 2.46 (s, 3H), 3.45–3.50 (m, 2H), 4.11 (t, 2H, J = 5.6 Hz), 7.36–7.38 (m, 2H), 7.78–7.80 (m, 2H); ^{13}C NMR (100 MHz, $CDCl_3$) δ 20.4, 30.4, 37.4, 68.2, 115.9, 120.9, 122.7, 139.7, 143.5, 157.8; HMRS (esi) m/z calcd for $C_{12}H_{15}F_3NO_4S$ [M+H] 326.0674 found 326.0681.

*4.1.3.2. 4-(2,2,2-trifluoroacetamido)butyl 4-methylbenzenesulfonate **(26)**.* Yellow solid, 60% yield; ^{1}H NMR (400 MHz, $CDCl_3$) δ 1.60–1.71 (m, 4H), 2.38 (s, 3H), 3.24–3.27 (m, 2H), 4.02 (t, 2H, J = 6.8 Hz), 7.29–7.33 (m, 2H), 7.68–7.63 (m, 2H); ^{13}C NMR (100 MHz, $CDCl_3$) δ 26.5, 29.6, 39.7, 69.3, 116.1, 120.6, 123.0, 139.9, 144.5, 157.9; HMRS (esi) m/z calcd for $C_{13}H_{17}F_3NO_4S$ [M+H] 340.0830, found 340.0839.

*4.1.4. General procedure for the synthesis of **27** and **28***

The appropriate diamine (10 eq) was dissolved in DCM and a solution of Boc_2O (1 eq) was added dropwise and the stirring was continued for 16 h at room temperature. Removal of the solvent gave residue that was dissolved in DCM and washed with brine (3 × 10 ml). The organic fraction was dried providing the desired products **27** and **28**.

*4.1.4.1. tert-Butyl (3-aminopropyl)carbamate **(27)**.* Yellow oil; 72% yield; ^{1}H NMR (400 MHz, $CDCl_3$) δ 1.40 (s, 9H), 1.80–1.85 (m, 2H) 2.00 (brs, 2H, exch D_2O), 2.61–2.68 (m, 2H), 2.90–2.98 (m, 2H), 5.90 (brs, 1H, exch D_2O); ^{13}C NMR (100 MHz, $CDCl_3$) δ 28.5, 33.3, 38.5, 39.4, 79.1, 156.4. HMRS (esi) m/z calcd for $C_8H_{19}N_2O_2$ [M+H] 175.1447, found 175.1441.

*4.1.4.2. tert-Butyl (4-aminobutyl)carbamate **(28)**.* Yellow oil; 60% yield; ^{1}H NMR (400 MHz, $CDCl_3$) δ 1.38 (s, 9H), 1.52–1.59 (m, 4H) 2.34 (brs, 2H, exch D_2O), 2.72–2.79 (m, 2H), 3.19–3.24 (m, 2H), 5.95 (brs, 1H, exch D_2O); ^{13}C NMR (100 MHz, $CDCl_3$) δ 27.6, 28.3, 30.7,

40.5, 41.8, 79.8, 156.5; HMRS (esi) *m/z* calcd for $C_9H_{21}N_2O_2$ [M+H] 189.1603, found 189.1610.

*4.1.5. General procedure for the synthesis of **29** and **30***

To a cooled solution (0 °C) of **25** or **26** (1 eq) respectively in THF was added a solution of **27** or **28** (1.5 eq) in THF. The reaction mixture was stirred for 6 h at 0 °C and then for 16 h at rt. Removal of the solvent gave a crude product that was purified by flash chromatography using as eluent a mixture of DCM/methanol/33% aqueous ammonia (9:1:0.05), providing the desired products **29** and **30**.

*4.1.5.1. tert-Butyl (4-((3-(2,2,2-trifluoroacetamido)propyl)amino) butyl)carbamate **(29)**.* Yellow oil, 35%yield; ^{1}H NMR (400 MHz, $CDCl_3$) δ 1.44 (s, 9H), 1.52–1.54 (m, 4H), 1.72–1.75 (m, 2H), 2.62–2.65 (m, 2H), 2.82–2.85 (m, 2H), 3.11 (m, 2H), 3.46–3.49 (m, 2H); ^{13}C NMR (100 MHz, $CDCl_3$) δ 27.1, 27.3, 28.0, 39.3, 40.2, 47.8, 48.8, 49.5, 78.7, 111.5, 114.4, 117.2, 120.1, 156.0, 156.8, 157.5; HMRS (esi) *m/z* calcd for $C_{14}H_{27}F_3N_3O_3$ [M+H] 342.2005, found 342.2015.

*4.1.5.2. tert-Butyl (3-((4-(2,2,2-trifluoroacetamido)butyl)amino)propyl)carbamate **(30)**.* Yellow oil, 47% yield; ^{1}H NMR (400 MHz, $CDCl_3$) δ 1.41 (s, 9H), 1.54–1.68 (m, 6H), 2.64 (t, 4H, J = 6.8 Hz), 3.07 (t, 2H, J = 6.4 Hz), 3.27–3.30 (m, 2H); ^{13}C NMR (100 MHz, $CDCl_3$) δ 25.7, 26.1, 26.4, 27.4, 28.8, 37.5, 39.0, 39.2, 78.5, 111.9, 114.7, 117.6, 120.4, 156.9, 157.2, 157.7, 158.0; HMRS (esi) *m/z* calcd for $C_{14}H_{27}F_3N_3O_3$ [M+H] 342.2005, found 342.2011.

*4.1.6. General procedure for the synthesis of **31** and **32***

To a stirred solution of **29** or **30** (1 eq) in Methanol was added slowly a solution of NaOH 40% p/p. The reaction mixture was allowed to stir at rt for 16 h. After removal of the solvent, the residual was taken up with DCM and washed with brine (3 × 10 ml). The organic layer was dried to obtain the desire products **31** and **32**.

*4.1.6.1. tert-Butyl (3-aminopropyl)(4-((tert-butoxycarbonyl)amino) butyl)carbamate **(31)**.* Yellow oil, 87% yield, ^{1}H NMR (400 MHz, D_2O) δ 1.28 (s, 18H), 1.32–1.35 (m, 4H), 1.44–1.52 (m, 2H), 2.41–2.52 (m, 6H), 2.93–2.94 (m, 2H); ^{13}C NMR (100 MHz, D_2O) δ 27.1.27.9, 28.2, 38.4, 39.9, 43.6, 46.3, 79.2, 155.7; HMRS (esi) *m/z* calcd for $C_{17}H_{36}N_3O_4$ [M+H] 346.2706, found 342.2709.

*4.1.6.2. tert-Butyl (4-aminobutyl)(3-((tert-butoxycarbonyl)amino) propyl)carbamate **(32)**.* Yellow oil, 64% yield; ^{1}H NMR (400 MHz, D_2O) δ 1.30 (s, 18H), 1.39–1.41 (m, 4H), 1.53–1.58 (m, 2H), 2.49–2.61 (m, 6H), 2.97–2.99 (t, 2H, J = 6.8 Hz); ^{13}C NMR (100 MHz, D_2O) δ 22.9, 23.5, 24.5, 25.6, 27.4, 38.5, 44.8, 46.5, 80.8, 157.9; HMRS (esi) *m/z* calcd for $C_{17}H_{36}N_3O_4$ [M+H] 346.2706, found 346.2714.

*4.1.7. General procedure for the synthesis of **35** and **36***

To a solution of **33** or **34** (5 eq) in toluene was added benzaldehyde (1 eq) and the resulting mixture was refluxed for 5 h. The solvent was removed in vacuo and the residue was taken up with ethanol. $NaBH_4$ (3 eq) was added and the solution was stirred for 12 h at room temperature. After evaporation of the solvent, the crude product was dissolved in DCM and washed with brine (2 × 10 ml). The organic phase was dried, evaporated and purified by flash chromatography using as eluent a mixture of DCM/methanol/33% aqueous ammonia (9:1:0.1), providing the desired products **35** and **36**.

*4.1.7.1. tert-Butyl (3-aminopropyl)(3-(benzylamino)propyl)carbamate **(35)**.* Yellow oil; 80% yield; ^{1}H NMR (400 MHz, $CDCl_3$) δ 1.41 (s, 9H), 1.74–1.77 (m, 4H), 2.61–2.65 (m, 2H), 2.73–2.78 (m, 2H), 3.13 (brs, 3H, exch D_2O), 3.21–3.27 (m, 4H), 3.81 (s, 2H), 7.29–7.32 (m, 5H); ESI-MS *m/z*: 322 $(M + H)^+$.

*4.1.7.2. tert-Butyl (4-((3-aminopropyl)(tert-butoxycarbonyl)amino) butyl)(3-(benzylamino)propyl) carbamate **(36)**.* Yellow oil, 81% yield; ^{1}H NMR (400 MHz, $CDCl_3$) δ 1.44 (s, 18H), 1.62–1.64 (m, 4H), 1.69–1.78 (m, 4H), 2.59 (t, 2H, J = 6.8 Hz), 2.66 (t, 2H, J = 6.6 Hz), 3.13–3.22 (m, 8H), 3.75 (s, 2H), 7.27–7.29 (m, 5H); ESI-MS *m/z*: 494 $(M + H)^+$.

*4.1.8. General procedure for the synthesis of **37** and **38***

To a stirred solution of **35** or **36** (1 eq) in methanol, Et_3N (1 eq) and ethyltrifluoroacetate (1 eq) were added and the stirring was continued for 16 h at room temperature. The solvent was removed and the crude product was purified by flash chromatography using as eluent a mixture of DCM/methanol/33% aqueous ammonia (9:1:0.05), providing the desired products **37** and **38**.

*4.1.8.1. tert-Butyl (3-(benzylamino)propyl)(3-(2,2,2-trifluoroacetamido)propyl)carbamate **(37)**.* Yellow oil, 72% yield; ^{1}H NMR (400 MHz, $CDCl_3$) δ 1.42 (s, 9H), 1.69–1.73 (m, 4H), 2.61 (t, 2H, J = 6.8 Hz), 3.18–3.20 (m, 2H), 3.27–3.29 (m, 4H), 3.76 (s, 2H), 7.29–7.31 (m, 5H); ESI-MS *m/z*: 418 $(M + H)^+$.

*4.1.8.2. tert-butyl(3-(benzylamino)propyl)(4-((tert-butoxycarbonyl)(3-(2,2,2-trifluoroacetamido) propyl)amino)butyl)carbamate **(38)**.* Yellow oil, 92% yield; ^{1}H NMR (400 MHz, $CDCl_3$) δ 1.44 (s, 18H), 1.46–1.48 (m, 6H), 1.67–1.70 (m, 4H), 2.62 (t, 2H, J = 7.0 Hz), 3.11–3.14 (m, 4H), 3.27–3.31 (m, 4H), 3.78 (s, 2H), 7.30–7.32 (m, 5H); ESI-MS *m/z*: 588 $(M + H)^+$.

*4.1.9. General procedure for the synthesis of **39** and **40***

37 or **38** (1 eq) was dissolved in THF, Et_3N (1 eq) and methyl iodide (1.5 eq) were added and the resulting mixture was stirred for 24 h h at room temperature. The solvent was removed under vacuum and the crude product was purified by flash chromatography using as eluent a mixture of DCM/methanol/33% aqueous ammonia (9:1:0.04), providing the desired products **39** and **40**.

*4.1.9.1. tert-butyl(3-(benzyl(methyl)amino)propyl)(3-(2,2,2-trifluoroacetamido)propyl)carbamate **(39)**.* Yellow oil, 66% yield; ^{1}H NMR (400 MHz, $CDCl_3$) δ 1.44 (s, 9H), 1.58–1.64 (m, 6H), 2.20 (s, 3H), 2.22–2.23 (m, 2H), 3.26–3.27 (m, 4H), 3.42 (s, 2H), 7.31–7.33 (m, 5H); ESI-MS *m/z*: 432 $(M + H)^+$.

*4.1.9.2. tert-butyl(3-(benzyl(methyl)amino)propyl)(4-((tert-butoxycarbonyl)(3-(2,2,2-trifluoroacetamido)propyl)amino)butyl)carbamate **(40)**.* Yellow oil, 30% yield; ^{1}H NMR (400 MHz, $CDCl_3$) δ 1.41 (s, 18H), 1.43–1.46 (m, 4H), 1.65–1.67 (m, 4H), 2.17 (s, 3H), 3.13–3.15 (m, 6H), 3.26–3.29 (m, 6H), 3.46 (s, 2H), 7.27–7.29 (m, 5H); ESI-MS *m/z*: 604 $(M + H)^+$.

*4.1.10. General procedure for the synthesis of **41** and **42***

To a stirred solution of **39 or 40** in methanol was added a solution of NaOH 40% p/p. The resulting mixture was allowed to stir for 16 h at room temperature. After removal of the solvent, the residue was dissolved in DCM and was washed with water (3 × 10 ml). The organic layer was dried providing the desire products **41** and **42**.

*4.1.10.1. tert-Butyl (3-aminopropyl)(3-(benzyl(methyl)amino)propyl) carbamate **(41)**.* Yellow oil, 88% yield; ^{1}H NMR (400 MHz, $CDCl_3$) δ 1.43 (s, 9H), 1.61–1.64 (m, 2H), 1.71–1.74 (m, 2H), 2.16 (s, 3H), 2.34 (t, 2H, J = 7.2 Hz), 2.67 (t, 2H, J = 6.6 Hz), 3.16–3.19 (m, 4H), 3.46 (s, 2H), 7.28–7.31 (m, 5H); ESI-MS *m/z*: 336 $(M + H)^+$.

*4.1.10.2. tert-butyl(4-((3-aminopropyl)(tert-butoxycarbonyl)amino) butyl)(3-(benzyl(methyl)amino) propyl)carbamate **(42)**.* Yellow solid, 92% yield; ^{1}H NMR (400 MHz, $CDCl_3$) δ 1.41 (s, 18H), 1.45–1.46 (m, 4H), 1.68–1.71 (m, 4H), 2.15 (s, 3H), 2.33 (t, 2H, J = 6.0 Hz), 2.73–2.75 (m, 2H), 3.00–3.03 (m, 4H), 3.12–3.15 (m, 4H), 3.44 (s, 2H), 7.21–7.27 (m, 5H); ESI-MS m/z: 508 $(M + H)^+$.

*4.1.11. General procedure for the synthesis of **43** and **44***

A solution of **41** or **42** dissolved in methanol, was hydrogenated over 10% Pd on charcoal under stirring for 2 h. After the consumption of the starting material, the solution was filtered in order to remove the catalyst and the solution was dried under vacuum. The crude product was purified by flash chromatography using as eluent a mixture of DCM/methanol/33% aqueous ammonia (8:2:0.2), providing the desired products **43** and **44**.

*4.1.11.1. tert-Butyll (3-aminopropyl)(3-(methylamino)propyl)carbamate **(43)**.* Yellow oil, 68% yield; ^{1}H NMR (400 MHz, $CDCl_3$) δ 1.40 (s, 9H), 1.61–1.69 (m, 4H), 1.72 (brs, 1H, exch D_2O), 2.38 (s, 3H), 2.56 (t, 2H, J = 6.6 Hz), 2.67 (t, 2H, J = 6.6 Hz), 3.16–3.23 (m, 4H); ESI-MS m/z: 246 $(M + H)^+$.

*4.1.11.2. tert-butyl(3-aminopropyl)(4-((tert-butoxycarbonyl)(3-(methylamino)propyl)amino)butyl) carbamate **(44)**.* Yellow oil, 76% yield; ^{1}H NMR (400 MHz, $CDCl_3$) δ 1.42 (s, 18H), 1.45–1.47 (m, 4H), 1.60–1.63 (m, 2H), 1.64–1.66 (m, 2H), 1.94 (brs, 3H, exch D_2O), 2.41 (s, 3H), 2.54–2.56 (m, 2H), 2.66 (t, 2H, J = 6.6 Hz), 3.14–3.22 (m, 8H); ESI-MS m/z: 418 $(M + H)^+$.

*4.1.12. General procedure for the synthesis of **49–59** and **17***

An equimolar mixture of the appropriate diamine **45–46** (1 eq), 1,4,5,8-naphthalene-tetracarbocylic dianhydride (1 eq) and (poly) amines **18–22**, **31**, **32**, **43**, **44**, **47** and **48** (1 eq) DMF was refluxed for 2 h. After cooling down, removal of the solvent gave residue that was purified by flash chromatography using as eluent a mixture of toluene/DCM/methanol/33% aqueous ammonia (4:5:1:0.03) providing the desired products **49–59** and **17**.

*4.1.12.1. tert-butyl(4-((tert-butoxycarbonyl)(3-((tert-butoxycarbonyl)amino)propyl)amino)butyl)(3-(7-(3-((2-methoxybenzyl) amino)propyl)-1,3,6,8-tetraoxo-3,6,7,8-tetrahydrobenzo[lmn][3,8] phenanthrolin –2(1H)-yl)propyl)carbamate **(49)**.* Brown oil; 15% yield; ^{1}H NMR (400 MHz, $CDCl_3$) δ 1.43 (s, 27H), 1.62–1.73 (m, 2H+1H exch D_2O), 1.95–2.01 (m, 4H), 2.71 (t, 2H, J = 6.4 Hz), 3.10–3.12 (m, 2H), 3.30–3.34 (m, 12H), 3.77 (s, 2H), 3.83 (s, 3H), 3.88–4.30 (m, 4H), 4.76 (brs, 1H, exch D_2O), 6.83–6.86 (t, 2H), 7.17–7.21 (m, 2H), 8.72–8.26 (m, 4H); ^{13}CNMR (100 MHz, $CDCl_3$) δ 25.4, 28.5, 28.1, 38.8, 39.2, 46.7, 48.9, 79.6, 106.5, 123.9, 126.3, 126.3, 126.9, 129.2, 130.9, 131.4, 142.4, 152.5, 153.9, 163.5; HMRS (esi) m/z calcd for $C_{50}H_{69}N_6O_{11}$ [M+H] 929.5024, found 929.5013.

*4.1.12.2. tert-butyl(4-((tert-butoxycarbonyl)(3-((tert-butoxycarbonyl)amino)propyl)amino)butyl)(3-(1,3,6,8-tetraoxo-7-(3-((2,3,4-trimethoxybenzyl)amino)propyl)-3,6,7,8-tetrahydrobenzo [lmn][3,8]phenanthrolin-2(1H)-yl)propyl)carbamate **(50)**.* Brown oil; 16% yield; ^{1}H.NMR (400 MHz, $CDCl_3$) δ 1.43 (s, 27H), 1.45–1.52 (m, 4H), 1.94–1.99 (m, 4H+1H exch D_2O), 2.74 (t, 2H, J = 6.8 Hz), 3.08–3.31 (m, 10H), 3.73 (s, 2H), 3.84 (s, 9H), 4.21 (t, 2H, J = 7.0 Hz), 4.29 (t, 2H, J = 7.2 Hz), 5.16 (brs, 1H, exch D_2O), 6.57 (d, 2H, J = 8.4 Hz), 6.92 (d, 2H, J = 8.4 Hz), 8.74 (s, 4H); ^{13}CNMR (100 MHz, $CDCl_3$) δ 25.7, 28.2, 28.4, 38.7, 39.0, 46.5, 48.6, 55.9, 60.7, 61.0, 79.4, 106.9, 123.9, 126.0, 126.4, 126.6, 128.9, 130.8, 130.9, 142.0, 152.9, 153.7, 162.8; HMRS (esi) m/z calcd for $C_{52}H_{73}N_6O_{13}$ [M+H] 989.5236, found 898.5230.

*4.1.12.3. tert-Butyl (3-((tert-butoxycarbonyl)amino)propyl)(3-(7-(3-((2-methoxybenzyl)amino)propyl)-1,3,6,8-tetraoxo-3,6,7,8-tetrahydrobenzo[lmn][3,8]phenanthrolin-2(1H)-yl)propyl)carbamate **(51)**.* Brown oil; 15% yield; ^{1}H NMR (400 MHz, $CDCl_3$) δ 1.43 (s, 18H), 1.62–1.73 (m, 2H+1H exch D_2O), 1.95–2.01 (m, 4H), 2.71 (t, 2H, J = 6.4 Hz), 3.10–3.12 (m, 2H), 3.30–3.34 (m, 4H), 3.77 (s, 2H), 3.83 (s, 3H), 3.88–4.30 (m, 4H), 4.76 (brs, 1H, exch D_2O), 6.83–6.86 (t, 2H, J = 7.2 Hz), 7.17–7.21 (m, 2H), 8.72–8.26 (m, 4H); ESI-MS m/z: 759 $(M + H)^+$.

*4.1.12.4. tert-butyl(4-((tert-butoxycarbonyl)amino)butyl)(3-(7-(3-((2-methoxybenzyl)amino)propyl)-1,3,6,8-tetraoxo-3,6,7,8-tetrahydrobenzo[lmn][3,8]phenanthrolin-2(1H)-yl)propyl)carbamate **(52)**.* Yellow oil, 19% yield; ^{1}H NMR (400 MHz, $CDCl_3$) δ 1.43 (s, 18H), 1.52–1.56 (m, 4H), 1.95–2.02 (m, 4H), 2.06 (brs, 1H, exch D_2O), 2.63–2.67 (m, 6H), 2.71–2.75 (m, 2H), 3.12 (brs, 1H, exch D_2O), 3.79 (s, 2H), 3.84 (s, 3H), 4.29 (t, 4H, J = 7.0 Hz), 6.84 (t, 2H, J = 7.4 Hz), 7.19 (t, 2H, J = 6.8 Hz), 8.73 (d, 4H, J = 7.2 Hz); ^{13}C NMR (100 MHz, $CDCl_3$) δ 27.2, 27.8, 28.1, 28.4, 29.6, 38.8, 39.0, 40.4, 46.4, 46.9, 48.9, 49.3, 55.2, 78.9, 110.1, 120.3, 126.4, 126.6, 128.0, 128.1, 129.7, 130.9, 130.9, 156.0, 157.5, 162.8, 162.9; ESI-MS m/z: 773 $(M + H)^+$.

*4.1.12.5. tert-butyl(3-((tert-butoxycarbonyl)amino)propyl)(4-(7-(3-((2-methoxybenzyl)amino)propyl)-1,3,6,8-tetraoxo-3,6,7,8-tetrahydrobenzo[lmn][3,8]phenanthrolin-2(1H)-yl)butyl)carbamate **(53)**.* Yellow oil; 15% yield; ^{1}H NMR (400 MHz, $CDCl_3$) δ 1.42 (s, 9H), 1.64–1.73 (m, 4H), 1.78–1.85 (m, 2H), 1.95–2.02 (m, 2H), 2.3 (brs, 1H, exch D_2O), 2.70–2.75 (m, 6H), 3.20–3.22 (m, 2H), 3.79 (s, 2H), 3.84 (s, 3H), 4.22 (t, 2H, J = 7.6 Hz), 4.29 (t, 2H, J = 6.4 Hz), 5.15 (brs, 1H exch D_2O), 6.84 (t, 2H, J = 7.2 Hz), 7.19 (t, 2H, J = 6.8 Hz), 8.73 (s, 4H). ^{13}C NMR (100 MHz, $CDCl_3$) δ 25.7, 27.0, 28.2, 28.4, 29.5, 38.9, 39.0, 40.5, 46.4, 47.4, 48.9, 49.1, 55.2, 79.0, 120.3, 126.5, 126.6, 128.0, 128.1, 129.7, 130.4, 130.9, 156.2, 157.5, 162.8; ESI-MS m/z: 773 $(M + H)^+$.

*4.1.12.6. tert-butyl(2-((tert-butoxycarbonyl)(3-(7-(3-((2-methoxybenzyl)amino)propyl)-1,3,6,8-tetraoxo-3,6,7,8-tetrahydrobenzo[lmn][3,8]phenanthrolin-2(1H)-yl)propyl)amino) ethyl)(3-((tert-butoxycarbonyl)amino)propyl)carbamate **(54)**.* Brown oil; 16% yield; NMR (200 MHz, $CDCl_3$) δ 1.46 (s, 27H), 1.66 (brs, 1H, exch D2O), 1.89–1.98 (m, 6H), 2.69–2.76 (t, 2H, J = 6.8 Hz), 2.88–3.26 (m, 10H), 3.78 (s, 2H), 3.84 (s, 3H), 4.20–4.32 (m, 4H), 5.12 (brs, 1H, exch D_2O), 6.81–6.88 (t, 2H, J = 7.0 Hz), 7.16–7.19 (t, 2H, J = 6.3 Hz), 8.74 (s, 4H); ESI-MS m/z: 902 $(M + H)^+$.

*4.1.12.7. tert-butyl(3-((tert-butoxycarbonyl)(3-((tert-butoxycarbonyl)amino)propyl)amino)propyl)(3-(7-(3-((2-methoxybenzyl) amino)propyl)-1,3,6,8-tetraoxo-3,6,7,8-tetrahydrobenzo [lmn][3,8] phenanthrolin-2(1H)-yl)propyl)carbamate **(55)**.* Brown oil; 20% yield; NMR (400 MHz, $CDCl_3$) δ 1.43 (s, 27H), 1.62–1.73 (m, 2H+1H exch D_2O), 1.95–2.01 (m, 2H), 2.71 (t, 2H, J = 6.4 Hz), 3.10–3.12 (m, 2H), 3.30–3.34 (m, 12H), 3.77 (s, 2H), 3.83 (s, 3H), 3.88–4.30 (m, 4H), 4.76 (brs, 1H, exch D_2O), 6.83–6.86 (t, 2H), 7.17–7.21 (m, 2H), 8.72–8.26 (m, 4H); HMRS (esi) m/z calcd for $C_{49}H_{66}N_6O_{11}$ [M+H] 914.4790, found 914.4797.

*4.1.12.8. tert-butyl(3-((tert-butoxycarbonyl)(methyl)amino)propyl)(3-(7-(3-((2-methoxybenzyl)amino) propyl)-1,3,6,8-tetraoxo-3,6,7,8-tetrahydrobenzo[lmn][3,8]phenanthrolin-2(1H)-yl)propyl) carbamate **(56)**.* Yellow oil; 16% yield; ^{1}H NMR (400 MHz, $CDCl_3$) δ 1.42 (s, 9H), 1.96–2.01 (m, 6H), 2.59 (s, 3H), 2.73 (t, 2H, J = 6.8 Hz), 2.85–2.88 (m, 2H), 3.23–3.35 (m, 4H), 3.80 (s, 2H), 3.82 (s, 3H), 4.17 (t, 2H, J = 7.6 Hz), 4.26 (t, 2H, J = 7.2 Hz), 6.81–6.83 (m, 2H), 7.18–7.24 (m, 3H), 8.72 (s, 4H); ESI-MS m/z: 773 $(M + H)^+$.

*4.1.12.9. tert-butyl(4-((tert-butoxycarbonyl)(3-(methylamino)propyl)amino)butyl)(3-(7-(3-((2-methoxybenzyl)amino)propyl)-1,3,6,8-tetraoxo-3,6,7,8-tetrahydrobenzo[lmn][3,8]phenanthrolin-2(1H)-yl) propyl)carbamate **(57)**.* Yellow oil; 23% yield; ^{1}H NMR (400 MHz, $CDCl_3$) δ 1.43 (s, 18H), 1.48–1.52 (m, 6H), 1.97–2.01 (m, 4H), 2.58 (s, 3H), 2.73 (t, 2H, J = 6.8), 2.77–2.79 (t, 2H), 3.09–3.27 (m, 8H), 3.80 (s, 2H), 3.83 (m, 3H), 4.15–4.19 (m, 2H), 4.28 (t, 2H, J = 6.8 Hz), 6.82–6.86 (m, 2H), 7.17–7.21 (m, 2H), 8.74 (s, 4H); ESI-MS m/z: 844 $(M + H)^+$.

*4.1.12.10. 2-(3-(4-(3-aminopropoxy)butoxy)propyl)-7-(3-((2-methoxybenzyl)amino)propyl)benzo[lmn] [3,8]phenanthroline-1,3,6,8(2H,7H)-tetraone **(58)**.* Brown oil; 26% yield; ^{1}H NMR (400 MHz, CDCl3) δ 1.41 (s, 9H), 1.53–1.54 (m, 4H), 1.70–1.72 (m, 2H), 1.89 (brs, 1H, exch D_2O), 1.93–2.03 (m, 4H), 2.70 (t, 2H, J = 6.8 Hz), 3.17–3.19 (m, 2H), 3.19–3.33 (m, 2H), 3.34–3.44 (m, 4H), 3.54 (t, 2H, J = 6.0 Hz), 3.76 (s, 2H), 3.81 (s, 3H), 4.25–4.31 (m, 4H), 4.99 (brs, 1H, exch D_2O), 6.81 (t, 2H, J = 8.0 Hz), 7.16 (t, 2H, J = 6.2 Hz), 8.69 (s, 4H); ^{13}C NMR (100 MHz, $CDCl_3$) δ 26.3, 26.4, 28.2, 28.3, 28.4, 28.7, 38.7, 39.1, 46.5, 49.0, 55.20, 68.7, 69.2, 70.6, 70.7, 77.4, 110.1, 120.3, 126.5, 126.6, 126.7, 128.1, 128.2, 129.7, 130.8, 130.8155.9, 157.6, 162.6, 162.8; HMRS (esi) m/z calcd for $C_{35}H_{43}N_4O_7$ [M+H] 631.3132, found 631.3139.

*4.1.12.11. tert-butyl(3-(7-(3-((2-methoxybenzyl)amino)propyl)-1,3,6,8-tetraoxo-3,6,7,8-tetrahydrobenzo[lmn][3,8]phenanthrolin-2(1H)-yl)propyl)carbamate **(59)**.* Yellow oil, 16% yield; ^{1}H NMR (400 MHz, $CDCl_3$) δ 1.44 (s, 9H), 1.94–1.97 (m, 4H), 2.72 (t, 2H, J = 7.0 Hz), 3.18–3.19 (m, 2H), 3.77 (s, 2H), 3.82 (s, 3H), 4.29 (t, 4H, J = 6.2 Hz); HMRS (esi) m/z calcd for $C_{33}H_{37}N_4O_7$ [M+H] 601.2662, found 601.2671.

*4.1.12.12. 2-Ethyl-7-(3-((2-methoxybenzyl)amino)propyl)benzo[lmn] [3,8]phenanthroline-1,3,6,8(2H,7H)-tetraone **(17)**.* Brown solid, quantitative yield, m.p. >250 °C; ^{1}H NMR (400 MHz, D_2O) δ 1.12 (t, 3H, J = 7.2 Hz), 2.01–2.05 (m, 4H), 3.00 (t, 2H, J = 7.4 Hz), 3.75 (s, 3H), 3.84–3.89 (m, 2H), 4.02 (t, 2H, J = 6.2 Hz), 4.13 (s, 2H), 6.73 (t, 1H, J = 7.4 Hz), 6.87 (d, 1H, J = 8.4 Hz), 7.15–7.19 (m, 2H), 8.15 (s, 4H). ^{13}C NMR (100 MHz, D_2O) δ 15.65, 26.74, 36.45, 45.51, 46.43, 54.77, 109.87, 117.37, 120.16, 123.79, 125.63, 130.25, 130.98, 155.83, 160.16; ESI-MS m/z: 473 (M + H).

*4.1.13. General procedure for the synthesis of **6**–**16***

To solution of **49**–**59** in methanol (20 ml), HCl 3 M (20 mL) was added and the resulting solution was stirred overnight at room temperature. Following solvent removal, the residue was washed with Et_2O (5 × 20 ml). The resulting solid was filtered and dried to afford **6**–**16** as hydrochloride salt.

*4.1.13.1. 2-(3-((4-((3-aminopropyl)amino)butyl)amino)propyl)-7-(3-((2-methoxybenzyl)amino)propyl)benzo[lmn][3,8]phenanthroline-1,3,6,8(2H,7H)-tetraone **(6)**.* Brown solid, quantitative yield; m.p. >250 °C; ^{1}H NMR (400 MHz, D_2O) δ 1.82–1.84 (m, 4H), 2.12–2.18 (m, 6H), 3.02–3.23 (m, 12H), 3.90 (s, 3H), 4.21–4.29 (m, 6H), 7.86 (t, 1H, J = 7.4), 7.04 (d, 1H, J = 8.2), 7.27–7.36 (m, 2H), 8.56–8.58 (m, 4H); ^{13}C NMR (100 MHz, D_2O) δ 22.8, 23.7, 24.0, 24.3, 24.8, 34.6, 36.7, 37.0, 37.7, 37.9, 44.1, 45.3, 46.6, 47.0, 55.5, 111.0, 118.1, 120.7, 125.0, 125.1, 125.2, 125.3, 130.9, 131.6, 157.6, 163.1, 163.2, 163.3; ESI-MS m/z: 315 $(M+2H)^{2+}$.

*4.1.13.2. 2-(3-((4-((3-aminopropyl)amino)butyl)amino)propyl)-7-(3-((2,3,4-trimethoxybenzyl)amino)propyl)benzo[lmn][3,8]phenanthroline-1,3,6,8(2H,7H)-tetraone **(7)**.* Brown solid, quantitative yield, m.p.>250 °C; ^{1}H NMR (400 MHz, D_2O) δ 1.81–1.85 (m, 4H), 2.07–2.16 (m, 6H), 3.10–3.21 (m, 12H), 3.69 (s, 3H), 3.74 (s, 3H), 3.92 (s, 3H), 3.19–3,24 (m, 6H), 6.74 (d, 1H, J = 9.2), 7.13 (d, 1H, J = 8.0), 8.42–8.47 (m, 4H); ^{13}C NMR (100 MHz, D_2O) δ 22.7, 23.7, 24.0, 24.2, 36.5, 37.6, 43.7,44.5, 45.3, 45.9, 47.0, 55.9, 60.7, 61.2, 107.9, 116.0, 125.4, 125.5, 125.6, 126.7, 130.9, 140.7, 151.8, 154.4, 163.5, 163.6; ESI-MS m/z: 345 $(M+2H)^{2+}$.

*4.1.13.3. 2-(3-((3-aminopropyl)amino)propyl)-7-(3-((2-methoxybenzyl)amino)propyl)benzo[lmn] [3,8]phenanthroline-1,3,6,8(2H,7H)-tetraone **(8)**.* Orange solid; quantitative yield; m.p. >250 °C; ^{1}H NMR (400 MHz, D_2O) δ 2.15-2-19 (m, 6H), 3.13–3.24 (m, 8H), 3.89 (s, 3H), 4.18–4.27 (m, 6H), 6.83 (t, 1H, J = 7.7), 7.01 (d, 1H, J = 8.2), 7.32–7.35 (m, 2H), 8.44–8.47 (m, 4H); ^{13}C NMR (100 MHz, D_2O) δ 23.7, 23.8, 24.3, 36.6, 36.7, 44.1, 44.7, 45.5, 55.6, 111.0, 118.0, 120.7, 125.0, 125.2, 130.9, 131.6, 157.6, 162.9, 163.0; ESI-MS m/z: 280 $(M+2H)^{2+}$.

*4.1.13.4. 2-(3-((4-aminobutyl)amino)propyl)-7-(3-((2-methoxybenzyl)amino)propyl)benzo[lmn] [3,8]phenanthroline-1,3,6,8(2H,7H)-tetraone **(9)**.* Brown solid; quantitative yield; m.p. >250 °C; ^{1}H NMR (400 MHz, D_2O) δ 1.62–1.68 (m, 4H), 2.00–2.04 (m, 4H), 2.91 (t, 2H, J = 7.0), 2.96–3.01 (m, 4H), 3.07 (t, 2H, J = 7.6), 3.74 (s, 3H), 4.03–4.10 (m, 4H), 4.13 (s, 2H), 6.71 (t, 1H, J = 8.2), 6.87 (d, 1H, J = 7.6), 7.13–7.19 (m, 2H), 8.34–8.36 (m, 4H); ^{13}C NMR (100 MHz, D_2O) δ 22.7, 23.8, 23.9, 24.2, 37.6, 37.8, 38.7, 44.0, 45.2, 46.6, 47.0, 55.4, 111.0, 118.0, 120.7, 125.1, 125.2, 125.3, 130.9, 131.5, 157.6, 163.2; ESI-MS m/z: 287 $(M+2H)^{2+}$.

*4.1.13.5. 2-(4-((4-aminobutyl)amino)butyl)-7-(3-((2-methoxybenzyl)amino)propyl)benzo[lmn][3,8]phenanthroline-1,3,6,8(2H,7H)-tetraone **(10)**.* Brown solid, quantitative yield, m.p. . >250 °C; ^{1}H NMR (400 MHz, D_2O) δ 1.84–2.11 (m, 4H), 2.12–2.21 (m, 4H), 3.11–3.22 (m, 8H), 3.90 (s, 3H), 4.24 (t, 2H, J = 7.0), 4.21 (t, 2H, J = 6.8), 4.29 (s, 2H), 6.88 (t, 1H, J = 7.6), 7.03 (d, 1H, J = 8), 8.49–8.50 (m, 4H); ^{13}C NMR (100 MHz, D_2O) δ 23.3, 23.7, 24.0, 24.2, 36.6, 37.6, 40.1, 44.0, 44.5, 46.7, 47.3, 55.4, 111.1, 118.1, 120.8, 125.1, 125.5, 130.8, 130.9, 131.6, 157.7, 163.2, 163.4; ESI-MS m/z: 287 $(M+2H)^{2+}$.

*4.1.13.6. 2-(3-((2-((3-aminopropyl)amino)ethyl)amino)propyl)-7-(3-((2-methoxybenzyl)amino) propyl)benzo[lmn][3,8]phenanthroline-1,3,6,8(2H,7H)-tetraone **(11)**.* Orange solid, quantitative yield; m.p. >250 °C; ^{1}H NMR (400 MHz, D_2O) δ 2.05–2.22 (m, 6H), 3.11–3.22 (m, 4H), 3.24–3.35 (m, 4H), 3.57 (s, 4H), 3.89 (s, 3H), 4.18 (t, 2H, J = 7.2), 4.23 (t, 4H, J = 6.8), 6.85 (t, 1H, J = 7.5), 7.02 (d, 1H, J = 8.1), 7.27–7.34 (m, 2H), 8.38–8.44 (m, 4H); ^{13}C NMR (100 MHz, D_2O) δ 23.6, 24.0, 24.3, 36.4, 37.6, 37.7, 43.2, 43.4, 44.0, 45.1, 46.0, 46.6, 55.4, 111.1, 118.1, 120.8, 125.5, 125.6, 131.0, 131.6, 157.7, 163.3; ESI-MS m/z: 302 $(M+2H)^{2+}$.

*4.1.13.7. 2-(3-((3-((3-aminopropyl)amino)propyl)amino)propyl)-7-(3-((2-methoxybenzyl)amino) propyl)benzo[lmn][3,8] phenanthroline-1,3,6,8(2H,7H)-tetraone **(12)**.* Brown solid, quantitative yield; m.p. >250 °C; ^{1}H NMR (400 MHz, D_2O) δ 2.07–2.18 (m, 6H), 3.09–3.25 (m, 12H), 3.88 (s, 3H), 4.18–4.78 (m, 6H), 6.86 (d, 1H, J = 7.4), 7.01 (d, 1H, J = 8.4), 7.24–7.41 (m, 2H), 8.37–8.52 (m, 4H); ESI-MS m/z: 308 $(M+2H)^{2+}$.

*4.1.13.8. 2-(3-((2-methoxybenzyl)amino)propyl)-7-(3-((3-(methylamino)propyl)amino)propyl)benzo [lmn][3,8]phenanthroline-1,3,6,8(2H,7H)-tetraone **(13)**.* Yellow solid, quantitative yield; m.p. >250 °C; ^{1}H NMR (400 MHz, D_2O) δ 2.15–2.21 (m, 6H), 3.12–3.35 (m, 11H), 3.89 (s, 3H), 4.18–4.48 (m, 6H), 6.86 (t, 1H, J = 7.5), 7.02 (d, 1H, J = 8.0), 7.30–7.34 (m, 2H), 8.50–8.59 (m, 4H); ^{13}C NMR (100 MHz, D_2O) δ 22.5, 24.0, 24.2, 32.8, 43.1, 44.0, 44.5, 45.4, 45.7, 46.7, 55.4, 63.5, 111.1, 118.1, 120.8, 125.5, 125.6, 131.0, 131.6, 157.7,

163.6; ESI-MS *m/z*: 287 $(M+2H)^{2+}$.

4.1.13.9. 2-(3-((2-methoxybenzyl)amino)propyl)-7-(3-((4-((3-(methylamino)propyl)amino)butyl) amino)propyl)benzo[lmn][3,8] phenanthroline-1,3,6,8(2H,7H)-tetraone ***(14)***. Brown solid, quantitative yield, m.p. >250 °C; ^{1}H NMR (400 MHz, D_2O) δ 1.81–1.83 (m, 4H), 2.11–2.21 (m, 6H), 2.76 (s, 3H), 3.14–3.25 (m, 12H), 3.90 (s, 3H), 4.23–4.29 (m, 6H), 6.85 (t, 1H, *J* = 7.6) 7.02 (d, 1H, *J* = 8.0), 8.66–8.72 (m, 4H); ^{13}C NMR (100 MHz, D_2O) δ 22.4, 22.7, 24.2, 32.8, 44.0, 44.4, 45.3, 45.7, 46.7, 46.9, 55.4, 110.1, 118.1, 120.8, 125.4, 125.6, 131.0, 131.6, 157.7, 163.6; ESI-MS *m/z*: 643 $(M + H)^+$.

4.1.13.10. 2-(3-(4-(3-aminopropoxy)butoxy)propyl)-7-(3-((2-methoxybenzyl)amino)propyl)benzo [lmn][3,8]phenanthroline-1,3,6,8(2H,7H)-tetraone ***(15)***. Orange solid, quantitative yield; m.p. 189–191 °C; ^{1}H NMR (400 MHz, D_2O) δ 1.47–1.49 (m, 4H), 1.89–1.95 (m, 4H), 2.17–2.22 (m, 2H), 3.89 (t, 2H, *J* = 7.4), 3.12 (t, 2H, *J* = 7.2), 3.40–3.48 (m, 4H), 3.54–3.62 (m, 4H), 3.89 (s, 3H), 4.10 (t, 2H, *J* = 6.9), 4.18 (t, 2H, *J* = 7.2) 4.28 (2, 2H), 6.86 (t, 1H, *J* = 7.6)7.01 (d, 1H, *J* = 8), 8.35–8.42 (m, 4H); ^{13}C NMR (100 MHz, D_2O) δ 23.9, 25.2, 26.5, 27.0, 37.4, 43.9, 46.4, 55.4, 67.5, 68.0, 70.2, 70.3, 110.9, 117.9, 120.6, 124.6, 124.8, 124.8, 124.9, 130.6, 130.8, 131.4, 131.5, 157.6, 162.3, 162.7.; ESI-MS *m/z*: 632 $(M + H)^+$.

4.1.13.11. 2-(3-aminopropyl)-7-(3-((2-methoxybenzyl)amino)propyl) benzo[lmn][3,8]phenanthroline-1,3,6,8(2H,7H)-tetraone ***(16)***. Yellow solid, quantitative yield, m.p. >250 °C; ^{1}H NMR (400 MHz, D_2O) δ 2.10–2.16 (m, 4H), 3.09–3.15 (m, 4H), 3.87 (t, 2H, *J* = 7.4), 3.87 (s, 3H), 4.15–4.22 (m, 4H), 4.25 (s, 2H), 6.84 (t, 1H, *J* = 7.6), 6.99 (d, 1H, *J* = 8.4), 7.25–7.30 (m, 2H), 8.44–8.50 (m, 4H); ^{13}C NMR (100 MHz, D_2O) δ 23.9, 25.3, 37.2, 37.5, 37.6, 37.8, 44.0, 46.5, 55.4, 110.9, 118.0, 120.7, 125.0, 125.1, 130.9, 131.5, 157.6, 163.1.; ESI-MS *m/z*: 502 $(M + H)^+$.

4.2. Biology

4.2.1. Fluorescence melting assay

Fluorescence melting curves were determined in a Roche LightCycler480 (λ_{ecc} 488 nm, λ_{em} 520 nm) in a total reaction volume of 20 μl containing 0.25 μM of the selected sequences (HTS: 5′Dabcyl-AGG GTT AGG GTT AGG GTT AGG GT-FAM 3′ and dsDNA: 5′-GGA TGT GAG TGT GAG TGT GAG GG-FAM 3′ previously annealed to its complementary strand 5′ Dabcyl CC CTC ACA CTC ACA CTC ACA TCC-3′) and increasing ligand concentrations in LiP buffer (10 mM LiOH, 50 mM KCl, pH 7.0 with H_3PO_4). In a typical experiment, samples were maintained at 30° for 5 min before being slowly heated to 95 °C (1 °C/min), kept at this temperature for 5 min and then annealed at the same rate. Recordings were taken during both the annealing and melting steps. Tm values were determined from the first derivatives of the melting profiles using the Roche LightCycler software. Each curve was repeated at least three times and errors were ±0.4 °C. ΔTm was calculated by subtracting the Tm value recorded in the presence of the ligand from the corresponding value in the absence of ligand. ΔΔTm represents the difference of ΔTm between the G-4 and dsDNA recorded at 2.5 μM ligand concentration.

4.2.2. Topoisomerase II

0.125 μg of pBR322 (*Inspiralis*) were incubated with increasing concentrations (0.5–100 μM) of tested compounds for 1 h h at 37 °C in the presence/absence of 1 U of human topoisomerase IIα (*Inspiralis*) in the required buffer. Reactions were stopped by the addition of loading buffer (10 mM Tris, 1 mM EDTA; 200 mM NaCl, bromophenol blue, xylene cyanol, pH 8.0) and the products were resolved on a 1% agarose gel in 1X TAE (10 mM Tris, 1 mM EDTA, 0.1% acetic acid pH 8.0, added of 0.1% SDS). The electrophoretic run was performed at 4.9 V/cm for 90 min min and finally the bands were stained with ethidium bromide (0.5 μg/ml in H_2O). When the topoisomerase cleavage activity was tested, the reaction was performed with 5 U of enzyme. Before loading, the reaction mixture was treated with proteinase K (1.6 μg), Na_2EDTA (12.5 mM) and SDS (0.5%) (*Sigma*), for 30 min min at 45 °C.

4.2.3. TAQ polymerase inhibition assay

The 1065–906 fragment of plasmid pBR322 (*Fermentas*) was amplified by PCR using the primers 3′GYRA (5′ TGA GGA TCC GCC TGG ACA GCA TGG 3′) and 5′GYRA (5′ GTC GAA TTC TCG GCG AGA AGC AGG 3′) at 0.5 μM concentration in the presence/absence of increasing concentrations of tested derivatives (0–20 μM) using 2.5 ng of plasmid and 2 U of *TAQ* polymerase enzyme (*Fermentas*). The reaction was carried out in an *Eppendorf* thermocycler by repeating the following PCR scheme for 25 cycles: 30 s at 94 °C; 30 s at 58 °C and 30 s at 72 °C. PCR products were resolved on a 2% agarose gel in 0.5 X TBE (4.2 V/cm for 1.5 h) stained by ethidium bromide and visualized on a *Geliance* apparatus.

4.2.4. Telomerase repeat amplification protocol assay (TRAP-lig)

Telomerase activity was monitored using a modified Telomere Repeat Amplification Protocol (TRAP) assay. 100 ng of substrate TS (5′ AAT CCG TCG AGC AGA GTT 3′) was elongated by the telomerase present in 5 μg of HeLa cells protein extract at 37 °C for 30 min in the presence/absence of increasing drug concentrations. Ligands were removed by QIA quick nucleotide purification extraction kit (Qiagen) and, after addition of 100 ng of reverse primer ACX (5′ GCG CGG CTT ACC CTT ACC CTT ACC CTA ACC 3′) and 2U *TAQ* polymerase, the amplification of the products was performed by PCR (33 cycles of 30 s at 92 °C, 30 s at 58 °C and 45 s at 72 °C). The reaction products were loaded onto a 10% polyacrylamide gel in 0.5x TBE and visualized by Sybr Green I staining (*Euroclone*).

4.2.5. Cell cultures

Jurkat T leukemia cells were purchased from ATCC (LGC Standard, Teddington, UK). Cells were grown in suspension and propagated in RPMI 1640 supplemented with 10% heat-inactivated bovine serum, 1% L-glutamine solution, and 1% penicillin/streptomycin (all purchased from Biochrom, Berlin, Germany). Cells were incubated at 37 °C, 5% CO2 and maintained in exponential growth by splitting the cultures every third day to a density of 0.5×10^6 cells.

4.2.6. Induction of apoptosis

After treatment with increasing concentrations of **8** or **9** (0.0–6.4 μM) for 24 h, cells were incubated with Guava Nexin Reagent (Merck Millipore, Hayward, CA, SA), containing 7-amino-actinomycin D and annexin V-phycoerythrin, for 20 min at room temperature in the dark and then analyzed *via* flow *cytometry.*

4.2.7. Caspase-3 activity

Activity of caspase-3 was evaluated with Caspase-3 Colorimetric Protease Assay Kit (Thermo Fisher Scientific, Carlsbad, CA, USA), according to manual instructions. Briefly, after 24 h treatment with increasing concentrations of **9** (0.0–6.4 μM), 3×10^6 cells/sample were washed in phosphate buffer 1x (PBS, Sigma Aldrich, St. Louis, MO, USA), re-suspended in Cell Lysis Buffer and kept on ice for 10 min. Cellular lysates were centrifuged at 10000 × g for 1 min. The supernatant was incubated for 2 h at 37 °C in the dark with 2x Reaction Buffer containing DTT 10 mM and 200 μM DEVD-pNA. The substrates are composed of the chromophore *p*-nitroanilide (pNA), and the synthetic tetrapeptide, DEVD (Asp-Glue-Val-Asp). Upon cleavage of the specific substrate by Caspase-3, free pNA light

absorbance was quantified at 405 nm, using the microplate reader Victor X3 (Perkin Elmer, Waltham, MA, USA), against a negative control processed such as the samples but without the DEVD addition to the reaction mixture. Caspase-3 activity was expressed as fold increase of treated cells respect to untreated cells. Cells treated with 100.0 μM valinomycin (Sigma Aldrich) for 1 h were used as positive control.

4.2.8. Analysis of PARP expression

The expression of the cleaved form of PARP was analyzed. After treatment with 8 or 9 (0.0–3.2 μM) for 24 h, 1×10^6 cells were fixed by 4% paraformaldehyde and permeabilized by using 90% ice-cold methanol. Cells were then incubated with the anti-cleaved PARP antibody labeled with fluorescein isothiocyanate (1:100, Thermo Fisher, Carlsbad, CA, USA). After washing, samples were analyzed *via* flow cytometry and the mean fluorescence was recorded.

4.2.9. Cell-cycle analysis

Cells were treated for 24 h with increasing concentrations of **8** or **9** (0.0–3.2 μM) and fixed in ice-cold ethanol. After washing, samples were incubated with Cell Cycle Reagent (Merck Millipore, Hayward, CA, SA) containing propidium iodide and incubated at room temperature in the dark for 30 min. Cells were then analyzed *via* flow cytometry.

4.2.10. Flow cytometry

All flow cytometric analyses were performed using Guava EasyCyte 6 2L cytometer (Guava Technologies, Merck Millipore). Approximately 5000 cells were evaluated for each sample.

4.2.11. Statistical analysis

Results are expressed as mean ± SEM of three experiments. Differences between treatments were assessed using one way ANOVA and Dunnett as post-test. All statistical analyses were performed using GraphPad InStat (GraphPad Prism, San Diego, CA, USA). $P < 0.05$ was considered significant.

4.3. Molecular modelling

4.3.1. DNA receptors preparation and optimization

The NMR structures of the 23-nt hybrid-1 (PDB code: 2JSM) [29] and 25-nt hybrid-2 (PDB code: 2JSL) [29] forms of the DNA G-quadruplex (G4-DNA) with the human telomeric sequence 5′-$TAG_3T_2AG_3T_2AG_3T_2AG_3$-3′ and 5′-$TAG_3T_2AG_3T_2AG_3T_2AG_3T_2$-3′ respectively, have been downloaded from the Protein Data Bank website [32]. Subsequently, the two telomeric sequences were modified in order to achieve the same 23-nt sequence 5′-$AG_3T_2AG_3T_2AG_3T_2AG_3$T-3′ of G4-DNA adopted in the biophysical studies using the graphical user interface of Maestro ver. 10.2 [33]. The so obtained hybrid-1 and hybrid-2 models were then treated with the Protein Preparation Wizard tool, all the hydrogen atoms added and the correct bond orders assigned. As concern the duplex DNA (dsDNA), we built the tridimensional model having the same experimental sequence using the graphical user interface of Maestro ver. 10.2 [33] and then submitted to Protein Preparation Wizard treatment [34]. Specifically, with the aim to maintain the intercalative binding site between the GC base pair, we choose as template structure the 6 pb crystallographic dsDNA (PDB code: 1Z3F) [35] complexed with the anticancer agent ellipticine and superimposed it with the GC base pair of the homology dsDNA (Fig. S1).

4.3.2. Molecular dynamics of G4-DNA and dsDNA

The previously prepared 23-nt G4-DNA receptors and the dsDNA have been submitted to Molecular Dynamics simulation using the NAMD 2.9 code [36]. The *parm99* Amber force field [37] including the recent *parmbsc0* nucleic acids parameters were used to treat the G4-DNA and dsDNA. The systems were placed in a 10.0 Å layer cubic water box using the TIP3P explicit water model and K^+ ions were added to neutralize the net charge. The SHAKE algorithm was applied to all covalent bonds involving hydrogen atoms and 2 fs integration time step was considered. The long-range electrostatic interactions were computed using the Particle Mesh Ewald (PME) method with a 1.0 Å grid spacing in periodic boundary conditions. All the receptors were thus subjected to a double minimization step using the conjugate gradient algorithm in the following conditions: *(i)* solvent and ions minimization, keeping all the solute fixed (2000 steps); *(ii)* minimization of the entire system, without any restriction (20000 steps). The minimized systems were equilibrated at 298.15 K through 5 ns in NVT ensemble followed by 5 ns of equilibration in NPT ensemble at 1 atm. Finally, a further equilibration step of 5 ns was performed in the NVE ensemble. Production run of 10 ns was performed in NPT conditions at 1 atm and 298.15 K while trajectory energies and coordinates were saved every 40 ps. Trajectories clusterization have been performed using the g-cluster tool of GROMACS ver. 4.5 [28] and the GROMOS algorithm using a RMSD cut-off of 0.2 nm.

4.3.3. Polyamine NDIs preparation

The 3D molecular structures of the most interesting **9**, **11** and **16** were built using the Maestro Build Panel ver. 10.2 [33] and all the hydrogen atoms were added. Their protonation state has been set according with that experimentally calculated at pH 7.0 revealing the ionization of all the primary and secondary aliphatic amine groups of both the spermine and spermidine-like side chains. Specifically, three amine groups were protonated for compounds **9**, four amine groups were ionized for compounds **11** and two amine groups for **16**. The so obtained NDI derivatives **9**, **11** and **16** were submitted to 3000 steps Polak-Ribiere conjugate gradient minimization (PRCG) (0.05 kJ/Å mol convergence threshold) with MacroModel ver. 10.8 [38] using the force field AMBER* and their conformational degrees of freedom were explored using the MC method. In particular, 10000 conformations were generated for each ligand and the GB/SA water implicit solvent model was considered. The total number of conformers identified for each ligand has been reported in Table S1 of the Supporting Information. In addition, conformers found within 3 kcal/mol above the global minimum were subjected to BASASA (Table S1), while only the energetically lowest conformer of each ligand (the global minimum) has been taken into account for docking calculations.

4.3.4. Docking setup

Molecular docking calculations against the hybrid-1 and hybrid-2 forms of G4-DNA human telomeric sequences and the experimental sequence of dsDNA were carried out using the AutoDock4.2 software package [30]. Ligands and both G4-DNA and dsDNA receptors were converted to apposite AD4 PDBQT file formats and the Gaisteiger–Marsili partial charges were then assigned. In order to explore the entire conformational space of both nucleic acids, the 3D grid box dimensions have been defined including the entire DNA macromolecules. Specifically, grid points of $126 \times 126 \times 126$ for the G4 DNA and of $70 \times 70 \times 70$ for the dsDNA with a 0.375 Å spacing were computed by mean of AutoGrid4.2. For each target, 100 docking poses were generated leaving other default docking parameters, only the rmsd tolerance (rmstol) was increased from the default value of 2.0 Å to 4.5 Å. Docking conformations were clustered on the basis of their rmsd. All the obtained complexes were subjected to a 3000 multi minimization phase using the AMBER* force field with MacroModel ver. 10.8 [30].

5. Associated content

Further Molecular Modelling analysis, complete compounds evaluation at the NCI 60 human cancer cell lines, elemental analysis and ^{1}H NMR and ^{13}C NMR spectra for selected compounds.

Acknowledgement

This work was supported by RFO (University of Bologna) and the Italian Ministry of Education (Funding for Investments of Base Research) (code FIRB-IDEAS RBID082ATK_002). We thank the National Cancer Institute (Bethesda, MD) for the anticancer assays. G.C. was supported by the UMG grant dedicated to the memory of Anna and Ninì Barbieri.

Appendix A. Supplementary data

Supplementary data related to this article can be found at http://dx.doi.org/10.1016/j.ejmech.2017.01.025.

References

[1] S.V. Bhosale, C.H. Jani, S.J. Langford, Chemistry of naphthalene diimides, Chem. Soc. Rev. 37 (2008) 331–342.
[2] Z. Hu, R.L. Arrowsmith, J.A. Tyson, V. Mirabello, H. Ge, I.M. Eggleston, S.W. Botchway, G.D. Pantos, S.I. Pascu, A fluorescent Arg-Gly-Asp (RGD) peptide-naphthalenediimide (NDI) conjugate for imaging integrin α(v)β(3) in vitro, Chem. Commun. (Camb) 51 (2015) 6901–6904.
[3] V. Tumiatti, A. Milelli, A. Minarini, M. Rosini, M.L. Bolognesi, M. Micco, V. Andrisano, M. Bartolini, F. Mancini, M. Recanatini, A. Cavalli, C. Melchiorre, Structure-activity relationships of acetylcholinesterase noncovalent inhibitors based on a polyamine backbone. 4. Further investigation on the inner spacer, J. Med. Chem. 51 (2008) 7308–7312.
[4] E. De Gianni, E. Turrini, A. Milelli, F. Maffei, M. Carini, A. Minarini, V. Tumiatti, T.D. Ros, M. Prato, C. Fimognari, Study of the cytotoxic effects of the new synthetic Isothiocyanate CM9 and its fullerene derivative on human T-leukemia cells, Toxins (Basel) 7 (2015) 535–552.
[5] Y. Wang, X. Zhang, J. Zhao, S. Xie, C. Wang, Nonhematotoxic naphthalene diimide modified by polyamine: synthesis and biological evaluation, J. Med. Chem. 55 (2012) 3502–3512.
[6] V. Tumiatti, A. Milelli, A. Minarini, M. Micco, A. Gasperi Campani, L. Roncuzzi, D. Baiocchi, J. Marinello, G. Capranico, M. Zini, C. Stefanelli, C. Melchiorre, Design, synthesis, and biological evaluation of substituted naphthalene imides and diimides as anticancer agent, J. Med. Chem. 52 (2009) 7873–7877.
[7] M.L. Bochman, K. Paeschke, V.A. Zakian, DNA secondary structures: stability and function of G-quadruplex structures, Nat. Rev. Genet. 13 (2012) 770–780.
[8] L.H. Hurley, DNA and its associated processes as targets for cancer therapy, Nat. Rev. Cancer 2 (2002) 188–200.
[9] S. Balasubramanian, S. Neidle, G-quadruplex nucleic acids as therapeutic targets, Curr. Opin. Chem. Biol. 13 (2009) 345–353.
[10] S. Balasubramanian, L.H. Hurley, S. Neidle, Targeting G-quadruplexes in gene promoters: a novel anticancer strategy? Nat. Rev. Drug Discov. 10 (2011) 261–275.
[11] G. Biffi, D. Tannahill, J. Miller, W.J. Howat, S. Balasubramanian, Elevated levels of G-quadruplex formation in human stomach and liver cancer tissues, PLoS One 9 (2014) e102711.
[12] S.A. Ohnmacht, S. Neidle, Small-molecule quadruplex-targeted drug discovery, Bioorg Med. Chem. Lett. 24 (2014) 2602–2612.
[13] F. Cuenca, O. Greciano, M. Gunaratnam, S. Haider, D. Munnur, R. Nanjunda, W.D. Wilson, S. Neidle, Tri- and tetra-substituted naphthalene diimides as potent G-quadruplex ligands, Bioorg Med. Chem. Lett. 18 (2008) 1668–1673.
[14] M. Gunaratnam, S. Swank, S.M. Haider, K. Galesa, A.P. Reszka, M. Beltran, F. Cuenca, J.A. Fletcher, S. Neidle, Targeting human gastrointestinal stromal tumor cells with a quadruplex-binding small molecule, J. Med. Chem. 52 (2009) 3774–3783.
[15] G.W. Collie, R. Promontorio, S.M. Hampel, M. Micco, S. Neidle, G.N. Parkinson, Structural basis for telomeric G-quadruplex targeting by naphthalene diimide ligands, J. Am. Chem. Soc. 134 (2012) 2723–2731.
[16] C. Marchetti, A. Minarini, V. Tumiatti, F. Moraca, L. Parrotta, S. Alcaro, R. Rigo, C. Sissi, M. Gunaratnam, S.A. Ohnmacht, S. Neidle, A. Milelli, Macrocyclic naphthalene diimides as G-quadruplex binders, Bioorg Med. Chem. 23 (2015) 3819–3830.
[17] S.L. Suraru, F. Würthner, Strategies for the synthesis of functional naphthalene diimides, Angew. Chem. Int. Ed. Engl. 53 (2014) 7428–7448.
[18] S.A. Ohnmacht, C. Marchetti, M. Gunaratnam, R.J. Besser, S.M. Haider, G. Di Vita, H.L. Lowe, M. Mellinas-Gomez, S. Diocou, M. Robson, J. Šponer, B. Islam, R.B. Pedley, J.A. Hartley, S. Neidle, A G-quadruplex-binding compound showing anti-tumour activity in an in vivo model for pancreatic cancer, Sci. Rep. 5 (2015) 11385.
[19] F. Doria, M. Nadai, M. Folini, M. Di Antonio, L. Germani, C. Percivalle, C. Sissi, N. Zaffaroni, S. Alcaro, A. Artese, S.N. Richter, M. Freccero, Hybrid ligand-alkylating agents targeting telomeric G-quadruplex structures, Org. Biomol. Chem. 10 (2012) 2798–2806.
[20] A. Milelli, V. Tumiatti, M. Micco, M. Rosini, G. Zuccari, L. Raffaghello, G. Bianchi, V. Pistoia, J. Fernando Díaz, B. Pera, C. Trigili, I. Barasoain, C. Musetti, M. Toniolo, C. Sissi, S. Alcaro, F. Moraca, M. Zini, C. Stefanelli, A. Minarini, Structure-activity relationships of novel substituted naphthalene diimides as anticancer agents, Eur. J. Med. Chem. 57 (2012) 417–428.
[21] M.A. Keniry, E.A. Owen, Insight into the molecular recognition of spermine by DNA quadruplexes from an NMR study of the association of spermine with the thrombin-binding aptamer, J. Mol. Recognit. 26 (2013) 308–317.
[22] H. Sun, J. Xiang, Y. Liu, L. Li, Q. Li, G. Xu, Y. Tang, A stabilizing and denaturing dual-effect for natural polyamines interacting with G-quadruplexes depending on concentration, Biochimie 93 (2011) 1351–1356.
[23] J.M. Barret, A. Kruczynski, S. Vispé, J.P. Annereau, V. Brel, Y. Guminski, J.G. Delcros, A. Lansiaux, N. Guilbaud, T. Imbert, C. Bailly, F14512, a potent antitumor agent targeting topoisomerase II vectored into cancer cells via the polyamine transport system, Cancer Res. 68 (2008) 9845–9853.
[24] E. Bonaiuto, A. Milelli, G. Cozza, V. Tumiatti, C. Marchetti, E. Agostinelli, C. Fimognari, P. Hrelia, A. Minarini, M.L. Di Paolo, Novel polyamine analogues: from substrates towards potential inhibitors of monoamine oxidases, Eur. J. Med. Chem. 70 (2013) 88–101.
[25] M. Micco, G.W. Collie, A.G. Dale, S.A. Ohnmacht, I. Pazitna, M. Gunaratnam, A.P. Reszka, S. Neidle, Structure-based design and evaluation of naphthalene diimide G-quadruplex ligands as telomere targeting agents in pancreatic cancer cells, J. Med. Chem. 56 (2013) 2959–2974.
[26] S. Alcaro, A. Artese, G. Costa, S. Distinto, F. Ortuso, L. Parrotta, Conformational studies and solvent-accessible surface area analysis of known selective DNA G-Quadruplex binders, Biochimie 93 (2011) 1267–1274.
[27] K.G. Xavier Daura, Bernhard Jaun, Dieter Seebach, Wilfred F. van Gunsteren, A.E. Mark, Peptide folding: when simulation meets experiment, Angew. Chem. - Int. Ed. 38 (1999) 236–240.
[28] S. Pronk, S. Páll, R. Schulz, P. Larsson, P. Bjelkmar, R. Apostolov, M.R. Shirts, J.C. Smith, P.M. Kasson, D. van der Spoel, B. Hess, E. Lindahl, GROMACS 4.5: a high-throughput and highly parallel open source molecular simulation toolkit, Bioinformatics 29 (2013) 845–854.
[29] A.T. Phan, V. Kuryavyi, K.N. Luu, D.J. Patel, Structure of two intramolecular G-quadruplexes formed by natural human telomere sequences in K+ solution, Nucleic Acids Res. 35 (2007) 6517–6525.
[30] G.M. Morris, R. Huey, W. Lindstrom, M.F. Sanner, R.K. Belew, D.S. Goodsell, A.J. Olson, AutoDock4 and AutoDockTools4: automated docking with selective receptor flexibility, J. Comput. Chem. 30 (2009) 2785–2791.
[31] V. MacroModel, Schrödinger, LLC, New, N. York, 2015.
[32] Protein Data Bank website. http://www.rcsb.org/.
[33] Maestro, Version 10.2, Schrödinger, LLC, New York, NY, 2015.
[34] Schrödinger Suite 2015-2 Protein Preparation Wizard; Epik version3.2, Schrödinger, LLC, New York, NY, 2015; Impact version 6.7, Schrödinger,LLC, New York, NY, 2015; Prime version 4.0, Schrödinger, LLC, New York, NY, 2015.
[35] A. Canals, M. Purciolas, J. Aymamí, M. Coll, The anticancer agent ellipticine unwinds DNA by intercalative binding in an orientation parallel to base pairs, Acta Crystallogr. D. Biol. Crystallogr. 61 (2005) 1009–1012.
[36] J.C. Phillips, R. Braun, W. Wang, J. Gumbart, E. Tajkhorshid, E. Villa, C. Chipot, R.D. Skeel, L. Kalé, K. Schulten, Scalable molecular dynamics with NAMD, J. Comput. Chem. 26 (2005) 1781–1802.
[37] A. Pérez, I. Marchán, D. Svozil, J. Sponer, T.E. Cheatham, C.A. Laughton, M. Orozco, Refinement of the AMBER force field for nucleic acids: improving the description of alpha/gamma conformers, Biophys. J. 92 (2007) 3817–3829.
[38] MacroModel, Version 10.8, Schrödinger, LLC, New York, NY, 2015.